A feedback loop between lamellipodial extension and HGF-ERK signaling specifies leader cells during collective cell migration

Author list and affiliations

Naoya Hino[1,2,18,*], Kimiya Matsuda[1], Yuya Jikko[3], Gembu Maryu[4], Katsuya Sakai[5,6], Ryu Imamura[5,6], Shinya Tsukiji[7,8], Kazuhiro Aoki[4,9,10], Kenta Terai[3], Tsuyoshi Hirashima[1,11,12], Xavier Trepat[13,14,15,16], Michiyuki Matsuda[1,3,17,*]

[1]Research Center for Dynamic Living Systems, Graduate School of Biostudies, Kyoto University, Sakyo-ku, Kyoto, 606-8501, Japan
[2]Institute of Science and Technology Austria, 3400 Klosterneuburg, Austria
[3]Department of Pathology and Biology of Diseases, Graduate School of Medicine, Kyoto University, Sakyo-ku, Kyoto 606-8501, Japan
[4]Division of Quantitative Biology, National Institute for Basic Biology, National Institutes of Natural Sciences, 5-1 Higashiyama, Myodaiji-cho, Okazaki, Aichi 444-8787, Japan.
[5]Division of Tumor Dynamics and Regulation, Cancer Research Institute, Kanazawa University, Kakuma, Kanazawa 920-1192, Japan
[6]WPI-Nano Life Science Institute (WPI-NanoLSI), Kanazawa University, Kakuma, Kanazawa 920-1192, Japan
[7]Department of Life Science and Applied Chemistry, Nagoya Institute of Technology, Gokiso-cho, Showa-ku, Nagoya 466-8555, Japan
[8]Department of Nanopharmaceutical Sciences, Nagoya Institute of Technology, Gokiso-cho, Showa-ku, Nagoya 466-8555, Japan
[9]Quantitative Biology Research Group, Exploratory Research Center on Life and Living Systems (ExCELLS), National Institutes of Natural Sciences, 5-1 Higashiyama, Myodaiji-cho, Okazaki, Aichi 444-8787, Japan
[10]Department of Basic Biology, School of Life Science, SOKENDAI (The Graduate University for Advanced Studies), 5-1 Higashiyama, Myodaiji-cho, Okazaki, Aichi 444-8787, Japan.
[11]The Hakubi Center, Kyoto University, Kyoto, Japan
[12]Japan Science and Technology Agency, PRESTO, Kawaguchi, Japan
[13]Institute for Bioengineering of Catalonia, Barcelona 08028, Spain
[14]Faculty of Medicine, University of Barcelona, Barcelona, Spain
[15]Institució Catalana de Recerca i Estudis Avançats (ICREA), Barcelona, Spain
[16]Center for Networked Biomedical Research on Bioengineering, Biomaterials and Nanomedicine (CIBER-BBN), Barcelona, Spain.
[17]Institute for Integrated Cell-Material Sciences, Kyoto University
[18]Lead Contact

***Corresponding authors:**
matsuda.michiyuki.2c@kyoto-u.ac.jp (M.M.), naoya.hino@ist.ac.at (N.H.)

Summary

Upon the initiation of collective cell migration, the cells at the free edge are specified as leader cells; however, the mechanism underlying the leader cell specification remains elusive. Here, we show that lamellipodial extension after the release from mechanical confinement causes sustained ERK activation and underlies the leader cell specification. Live-imaging of MDCK cells and mouse epidermis with FRET-based biosensors showed that leader cells exhibit sustained ERK activation in an HGF-dependent manner. Meanwhile, follower cells exhibit oscillatory ERK activation waves in an EGF signaling-dependent manner. Lamellipodial extension at the free edge increases the cellular sensitivity to HGF. The HGF-dependent ERK activation, in turn, promotes lamellipodial extension, thereby forming a positive feedback loop between cell extension and ERK activation, and specifying the cells at the free edge as the leader cells. Our findings show that the integration of physical and biochemical cues underlies the leader cell specification during collective cell migration.

Keywords

Collective cell migration, leader cell specification, ERK, HGF, lamellipodia, feedback regulation, FRET

Introduction

For spatio-temporally organized cell specification, cells sense the surrounding environment through biochemical factors including growth factors, cytokines, and hormones. It has also been shown that cells sense mechanical cues such as cell stretch, substrate stiffness, and fluid flow, which modulate intracellular signaling activity and thereby cell functions (Jansen et al., 2015; Vining and Mooney, 2017). Although each of the regulatory mechanisms has been extensively studied, less is known about whether and how the interplay between biochemical and mechanical cues regulate the cell specification (Chan et al., 2017).

Collective cell migration, the cohesive movement of a cell cluster, is involved in embryonic development, wound healing, cancer metastasis, etc. (Friedl and Gilmour, 2009; Mayor and Etienne-Manneville, 2016). Upon the initiation of collective cell migration, leader cells, which can be recognized by large lamellipodial protrusions, arise at the free edge of the epithelial cell sheets. These leader cells instruct follower cells and dictate the direction of cohesive cell movement (Khalil and Friedl, 2010; Mayor and Etienne-Manneville, 2016). The leader cells also provide a major driving force for guiding collective cell migration (Trepat et al., 2009), and these properties require integrin-mediated cell-substrate adhesion in conjunction with Rac1-mediated lamellipodial protrusion (Yamaguchi et al., 2015). Meanwhile, the generation of the leader cells is negatively regulated by RhoA and downstream myosin contraction as well as lateral inhibition through Notch1-Dll4 (Omelchenko et al., 2003; Reffay et al., 2014; Riahi et al., 2015). However, the molecular mechanisms underlying the leader cell specification at the onset of collective cell migration remain elusive.

Hepatocyte growth factor (HGF) is predominantly produced by mesenchymal stromal cells and binds to the Met receptor tyrosine kinase on various cell types in paracrine and endocrine manners (Nakamura and Mizuno, 2010; Viticchie and Muller, 2015). HGF-binding induces auto-phosphorylation of Met, and thereby activates multiple signaling cascades, including mitogen-activated protein kinase cascades. The Met-activated signaling cascades promote cell proliferation, survival, and migration. The function of HGF on epithelial morphogenesis has been extensively studied by using Madin-Darby canine kidney (MDCK) epithelial cells. HGF is also known as scatter factor (SF), and induces MDCK cell scattering (Stoker et al., 1987). Furthermore, HGF induces the tubulogenesis of MDCK cells in 3D culture (Montesano et al., 1991b). However, less is known about how HGF regulates collective cell migration despite its critical role in wound healing (Chmielowiec et al., 2007; Li et al., 2013; Miura et al., 2017).

During collective cell migration, activation waves of extracellular signal-regulated kinase (ERK) are repeatedly propagated from the leader cells to the follower cells (Aoki et al., 2017; Hiratsuka et al., 2015; Matsubayashi et al., 2004). This ERK activation waves are coupled with mechanical force generation (Boocock et al., 2020; Hino et al., 2020), and direct front-rear polarity of the follower cells, leading to long-distance coordinated cell migration (Das et al., 2015; Tambe et al., 2011). The intercellular propagation of ERK activation in epithelial cells depends on epidermal growth factor receptor (EGFR) family proteins and a disintegrin and metalloprotease 17 (ADAM17)-mediated shedding of EGFR ligands, which

are collectively called the EGF-EGFR signaling pathway (Aoki et al., 2017; Aoki et al., 2013; Lin et al., 2022).

An important question to be addressed is how ERK activation is implicated in the leader cell specification because the previous studies mostly focused on the role of ERK activation in the follower cells, and the leader cells are also a significant factor organizing the collective cell migration. Here, by using MDCK cells and mice expressing Förster resonance energy transfer (FRET)-based biosensors for ERK and Ras (Harvey et al., 2008; Komatsu et al., 2011; Lin et al., 2022; Mochizuki et al., 2001), we show that the release of mechanical confinement imposed by cell crowding or physical barriers increases cellular sensitivity to hepatocyte growth factor (HGF) and thereby specifies cells facing the free edge as the leader cells of the collective cell migration. Our study clarifies that biochemical cues and physical environment cooperatively regulate the generation of the leader cells at the free edge of the epithelial cell sheets.

Results

Leader cells show sustained ERK activation independently of EGFR activity

During collective migration of epithelial cells, ERK activation waves are originated from leader cells and organizes the coordinated movement. To characterize this phenomenon, we used MDCK cells expressing a FRET biosensor, EKARrEV-NLS, with which ERK activity can be monitored by the FRET/CFP fluorescence ratio (Komatsu et al., 2011; Lin et al., 2022). The cells were seeded in a culture insert placed on a collagen-coated glass substrate (Figure 1A). After 20 hr of incubation, the culture insert was removed, allowing monolayer expansion by collective cell migration. As reported previously, migrating MDCK cells exhibited ERK activation waves, which emanated from the leader cells and propagated toward the follower cells repeatedly (Figures 1B, 1C, and Video S1) (Aoki et al., 2017; Hino et al., 2020). Here, we defined the leader cells as cells facing a free edge after the removal of the culture insert (Figure 1A). During collective cell migration, the leader cell positions are occasionally overtaken by the following cells. Therefore, to continuously monitor the ERK activity in the leader cells, we employed a region-based analysis, in which the FRET/CFP ratio at the free edge of the epithelial cell sheet in the kymographs was defined as ERK activity in the leader cell region (Figure S1A). Also, the FRET/CFP ratio at the region 200 μm distant from the free edge was defined as the ERK activity in the follower cells. This analysis clearly shows that the leader cells exhibit sustained ERK activation while the follower cells show oscillatory ERK activation caused by the wave propagation (Figures 1B–1E, S2A, and S2B). Note that the sustained ERK activity in leader cells was also observed by single cell tracking of ERK activity, negating the possibility that the sustained high values were due to the averaging of a few cells during the region-based analysis (Figures S2C and S2D). As we have previously shown (Aoki et al., 2017; Aoki et al., 2013; Hino et al., 2020), the ERK activity in the follower cells was markedly suppressed by an EGFR inhibitor, PD153035. Surprisingly, however, the effect of PD153035 was modest in the leader cells (Figures 1F–H and Video S2). Thus, unlike the follower cells, the leader cells possess a mechanism to exhibit the sustained ERK activation in an EGFR-independent manner.

HGF triggers sustained ERK activation in the leader cells

If not EGFR, which signaling pathway is responsible for the sustained ERK activation in the leader cells? MDCK cells exhibit the pulsatile ERK activation in the absence of fetal bovine serum (FBS), because MDCK cells produce EGFR ligands (Lin et al., 2022). However, we noticed that FBS is required for the sustained ERK activation in the presence of the EGFR inhibitor (Figures 2A–2C and Video S3), suggesting that molecule(s) in FBS cause the sustained ERK activation in the leader cells. We next tested HGF because of its significant role in motogenesis and morphogenesis of epithelial cells (Montesano et al., 1991a; Montesano et al., 1991b; Stoker et al., 1987). Interestingly, HGF induced sustained ERK activation in the leader cells, but not the follower cells, in the presence of the EGFR inhibitor (Figures 2D–2F). In this experiment, ERK activation in each cell was also confirmed by a single cell-based method (Figures 2G and S1B). Importantly, the effect of HGF can also be

seen in the absence of the EGFR inhibitor (Figures S2E-S2I). Moreover, CRISPR/Cas9-mediated knock-out (KO) of the HGF receptor Met (*MET*) abrogated the sustained ERK activation in the leader cells cultured in FBS-containing medium (Figures 2H–2J and Video S4). A similar observation was obtained in two independent Met KO clones (Figure 2K), confirming that the HGF-Met signaling pathway causes sustained ERK activation in the leader cells.

To what extent does the confinement release assay of MDCK cells recapitulate the collective cell migration of epithelial cells *in vivo*? To answer this question, we observed the ERK activity of mice expressing hyBRET-EKAREV-NES (Komatsu et al., 2018), a cytosolic ERK activity reporter, under a two-photon excitation microscope (Figure 2L). We previously reported that ERK activation waves promote wound healing of the mouse ear skin (Hiratsuka et al., 2015; Sano et al., 2018). The EGFR inhibitor erlotinib suppressed ERK activity in the follower cells as expected (Figure 2M and 2N). By contrast, the leader cells retained high ERK activity even after the EGFR inhibitor treatment. This high ERK activity in the leader cells was abolished by subsequent administration of the Met inhibitor glumetinib. Thus, the HGF-Met signaling pathway causes sustained ERK activation in the leader cells during wound healing *in vivo* as in the confinement release assay of MDCK cells.

The HGF-Met signaling pathway is activated primarily in the leader cells despite similar Met expression level to the follower cells

We next asked why the HGF-Met signal causes sustained ERK activation primarily in the leader cells. We did not find a significant difference either in the total amount or subcellular localization of Met between the leader and the follower cells (Figures 3A–3C). A previous report showed that the HGF binding to cells depends on cell density (Mizuno et al., 1993). In line with this, we found that HGF activated Met and ERK robustly in sparse cells, but only modestly in confluent cells (Figures S3A–S3G). Thus, we speculated that the difference in the HGF binding might have caused the difference in responsiveness between the leader and follower cells. To examine this idea, we visualized HGF-Met binding and subsequent endocytosis by using fluorescently labeled recombinant HGF. Five and a half hours after the addition of the recombinant HGF, HGF intensity was high in the leader cells and low in the follower cells (Figures 3D and 3E). The cell area, which inversely correlates with the cell density, was also higher in the leader cells than in the follower cells (Figures 3D and 3F). Similarly, the HGF-induced ERK activation was high in the leader cells with a gradual decrease in a distance-dependent manner (Figures 3D and 3G). Indeed, the ERK activity in each cell correlated with HGF intensity and the cell area (Figures 3H and 3I), suggesting a close relationship among HGF intensity, cell area, and ERK activity. Furthermore, the HGF intensity in the leader cells was decreased by inhibitors of dynamin-dependent endocytosis or Met tyrosine kinase activity (Figures 3J–3L), suggesting that HGF is endocytosed upon Met activation primarily in the leader cells. However, the endocytosis inhibitor treatment did not suppress the ERK activity in the leader cells but rather increased slightly (Figures S4A and S4B), likely by preventing Met from endocytosis-mediated downregulation (Hammond et al., 2003). These results show that the increased HGF intensity in the leader cells is not the cause

of the leader cell-specific HGF-Met-ERK activation, but rather the consequence of Met activation and subsequent endocytosis.

We further investigated whether the binding of HGF on cell surface is different between leader and follower cells. Here, we examined the HGF binding to the cell surface under the condition in which endocytosis was inhibited on ice. Interestingly, there was no obvious difference in the binding of HGF to cell surface between the leader and the follower cells (Figure S4C). Please note that we used high concentration HGF (20 ng mL^{-1}) in this experiment because the fluorescence was not detectable with low HGF concentrations. Collectively, we conclude that the HGF-Met signaling pathway is primarily activated in the leader cells despite similar Met expression level and HGF-binding affinity to the follower cells.

HGF activates Ras at the lamellipodia of leader cells

To gain further insight into the mechanism of the leader cell-specific ERK activation, we examined the subcellular activation of Ras, which represents the activation area of upstream receptor tyrosine kinases (Sawano et al., 2002). To this end, we used another FRET biosensor, Raichu-Ras (Mochizuki et al., 2001). MDCK cells with Raichu-Ras were co-cultured with those without the biosensor to visualize the Ras activity in the migrating cell cluster discretely. As anticipated, leader cells exhibited higher Ras activity than the follower cells in an HGF-dependent manner (Figures 4A, 4B, and Video S5). More importantly, we found that Ras was activated mainly in the lamellipodia of the leader cells (Figures 4A and 4C). By contrast, the follower cells did not show such a subcellular bias of the Ras activity. These results imply that the Met activation is also biased to the lamellipodial protrusion of the leader cells.

Lamellipodial extension after the release from mechanical confinement increases the HGF sensitivity of leader cells

Because HGF-dependent Ras activation is specifically observed in the lamellipodia of the leader cells facing the free edge, we speculated that loss of cell-cell junctions might be important for the HGF-dependent ERK activation in leader cells. The regulation of HGF-Ras-ERK activation by the cell-cell junction formation is reminiscent of contact inhibition of cell growth (Li et al., 2004; Machide et al., 2006). Given that the cell-cell junction is a central regulator of contact inhibition (Mendonsa et al., 2018), we disrupted the adherens junction (AJ) by CRISPR/Cas9-mediated KO of α-1-catenin (*CTNNA1*), an essential factor for AJ formation (Hino et al., 2020). Against our expectation, in α-1-catenin KO cells the difference in ERK activity between the leader cells and the follower cells was still clearly maintained (Figures 5A–5D and Video S6), indicating that the cell-cell junctions are not the direct regulator of the HGF sensitivity. Importantly, frequency of sporadic ERK activation is increased in the α-1-catenin KO cells (Video S6), which might be due to the increased cryptic lamellipodium formation in the follower cells of α-1-catenin KO cells as reported previously (Ozawa et al., 2020). These results raise the possibility that not loss of cell-cell interaction but

lamellipodial extension is a crucial regulator of the HGF sensitivity. This idea is in line with the clear correlation between cell area and ERK activation (Figure 3F). We have shown that stretch-dependent ERK activation is completely inhibited by the EGFR inhibitor (Hino et al., 2020), suggesting that passive cell area increase is not sufficient for the HGF-dependent ERK activation. Thus, we hypothesized that the lamellipodial protrusion toward the free space increases the cellular sensitivity to HGF. To test this hypothesis, we seeded cells in a silicone confinement to suppress the lamellipodial protrusions. When cells were released for migration by removing the confinement, the leader cells showed higher ERK activity than follower cells in the presence of HGF and EGFR inhibitor (Figure 5E and 5F). By contrast, without removing the confinement, the ERK activity of the cells facing the confinement was similar to that of the follower cells and lower than that of the released leader cells (Figures 5E, 5F, and Video S7), indicating that the suppression of cell protrusion by a physical barrier inhibits ERK activation in leader cells. Furthermore, inhibition of lamellipodial extension with inhibitors of the Arp2/3 complex, CK666, or of actin polymerization, Latrunculin A, also suppressed ERK activation in the leader cells (Figures 5G, 5H, and S5A–S5C). These observations indicate that the lamellipodial extension is indispensable for the HGF-dependent sustained ERK activation in the leader cells.

To directly study the role of the lamellipodial protrusion in the HGF-dependent ERK activation, we induced lamellipodia in the follower cells by using self-localizing ligand-induced protein translocation (SLIPT) approach (Suzuki et al., 2022). With the SLIPT system, m^{D}cTMP treatment triggers translocation of ^{iK6}DHFR fused with DH-PH domain of Tiam1, a Rac1 guanine nucleotide exchange factor (GEF), to the plasma membrane, thereby leading to Rac1 activation (Figure 5J). Here, the cells expressing miRFP703-tagged ^{iK6}DHFR-Tiam1 (DH-PH) and the plasma membrane marker mCherrry-HRasCT were mixed with parent cells to discretely visualize the morphology of the target cells. As anticipated, m^{D}cTMP induced the translocation of ^{iK6}DHFR-Tiam1 (DH-PH) to the plasma membrane and caused lamellipodial protrusion (Figure 5I). In the absence of HGF, the m^{D}cTMP treatment failed to increase ERK activity in the follower cell (Figures 5I and 5K). By contrast, in the presence of HGF, the m^{D}cTMP treatment triggered ERK activation in the lamellipodia-induced cells but not the surrounding control cells. This result indicates that lamellipodial protrusion sensitize cells to HGF. Note that the ERK activation after the m^{D}cTM treatment was attenuated in 1 hr. This might be because of the modest lamellipodial protrusions imposed by the cell crowding, and/or the lack of front-rear polarization of Rac1 activation that is seen in leader cells (Yamaguchi et al., 2015).

Talin1-mediated immature focal complex is required for the HGF-dependent sustained ERK activation

Knowing the importance of lamellipodial extension, we asked whether cell-substrate contacts through focal adhesions also play a role in the HGF-dependent ERK activation in the leader cells. To this end, we quantified paxillin, a major focal adhesion (FA) protein, and the active phospho-ERK protein (pERK) by immunostaining (Figure 6A). The paxillin-positive FA intensity was highest in leader cells and decreased rapidly as the cells drew apart from the

leader cells, regardless of HGF (Figure 6B). The pERK was also highest at the leader cells and decreased in a similar manner as the FAs (Figure 6C); however, in stark contrast to the FAs, pERK enrichment at the leader cells was not observed in the absence of HGF. The pERK intensity in each cell was positively correlated with the FA intensity in a manner dependent on HGF treatment (Figures 6D and 6E). These observations give rise to the possibility that FAs are indispensable for the HGF-dependent ERK activation at the leader cells. To test this model, we knocked out talin1 (*TLN1*), which plays a pivotal role in FA formation. The cell area and the FA intensity of talin1 KO cells were markedly less than those of the WT cells (Figures S6A–S6C). Moreover, the HGF-dependent ERK activation in the leader cells was suppressed in the talin1 KO cells, indicating that talin1 plays an essential role in the HGF sensitivity (Figures 6F, 6G, and Video S8). We next examined the effect of a ROCK inhibitor in leader cells, because actomyosin contraction by Rho-ROCK signaling activation is indispensable for the maturation of FAs (Burridge and Guilluy, 2016). Against our expectation, however, the ROCK inhibitor did not significantly alter the ERK activity in leader cells (Figures 6H and 6I)), although the formation of FAs was suppressed as expected (Figures S6D and S6E). These results indicate that the talin1-dependent formation of immature focal complexes is indispensable for the HGF-dependent ERK activation, but the force-dependent maturation of FAs is dispensable. Given that talin1 KO abrogates cell spreading (Figures S6A and S6B) and that lamellipodial protrusions determines the HGF sensitivity (Figure 5), we concluded that talin1-mediated immature focal complex formation is a prerequisite for the leader cell-specific HGF sensitivity.

As a potential mechanism to associate lamellipodial protrusions with the HGF-Met signaling, we speculated that lamellipodia may promotes the clustering of the HGF-Met complex, leading to Met auto-phosphorylation. Lamellipodial protrusions are enriched with lipid rafts (Kim et al., 2011; Manes et al., 1999), and some heparan sulfate proteoglycans (HSPGs) are localized to lipid rafts (Gutierrez et al., 2014; Tkachenko and Simons, 2002). HSPGs bind to various growth factors including FGF, HGF, and HB-EGF. Thus, the clustering of HSPG-HGF-Met complex at the lipid rafts in lamellipodia might account for the leader cell-specific signal activation. In accordance with this hypothesis, surfen, which prevents growth factors from binding to HSPGs, significantly suppressed the sustained ERK activation in leader cells (Figures S6F and S6G). Collectively, these results showed that, lamellipodial extension toward the free space built on the talin1-dependent focal complexes bestows the HGF sensitivity on the leader cells in an HSPG-dependent manner.

ERK activation in leader cells triggers lamellipodial protrusion of the leader cells and increases traction force

Finally, we sought to determine the function of the sustained ERK activation in the leader cells. Leader cells exhibit prominent traction force generation with large lamellipodial protrusions (Trepat et al., 2009; Yamaguchi et al., 2015). Thus, we examined whether ERK activation is implicated in these leader cell properties. First, to see the effect of ERK activation on leader cell morphology, we employed MDCK cells expressing 2paRAF, an optogenetic tool for ERK activation (Aoki et al., 2013; Kinjo et al., 2019). 2paRaf consists of

the membrane-targeted CIBN-mScarlet-I fusion protein and the BFP-CRY2-Raf1 fusion protein. Upon blue light illumination, the BFP-CRY2-Raf1 binds to the CIBN, thereby leading to Raf1 and downstream ERK activation. Under the condition in which the cell-autonomous ERK activation was suppressed with an EGFR inhibitor and serum depletion, light-induced ERK activation robustly induced lamellipodial protrusion (Figures 7A, 7B, and Video S9). This effect was canceled by a MEK inhibitor, trametinib, or an Arp2/3 inhibitor, CK666, indicating that ERK activation induces lamellipodial protrusions in an Arp2/3-dependent manner.

We next employed traction force microscopy to explore how HGF treatment affects the traction force generation by the leader cells (Trepat et al., 2009). HGF increased the traction force that was parallel (X-traction) to the direction of collective cell migration (Figure 7C and 7D). On the other hand, the generation of traction force perpendicular to the direction of the collective cell migration (Y-traction) was less promoted by HGF treatment (Figure 7C and 7E). These results indicate that HGF treatment promotes traction force generation, thereby contributing to the driving force of the collective cell migration. Collectively, our findings showed that HGF-mediated signal activation in leader cells is crucial for acquisition of the leader cell properties to guide collective cell migration.

Discussion

We found that the leader cells and the follower cells show distinct ERK activity dynamics, i.e., sustained and oscillatory ERK activations, respectively (Figure 1). The sustained ERK activation in the leader cells depends on the HGF-Met signaling pathway, while the oscillatory ERK activation in the follower cells depends on the EGF-EGFR signaling pathway (Figure 2). Release from mechanical confinement increase cellular HGF sensitivity in a manner dependent on lamellipodial extension and talin1-mediated focal complexes (Figures 5 and 6). This property underlies sustained ERK activation in the leader cells, leading to the formation of lamellipodial protrusions and traction force generation, i.e., leader cell specification (Figure 7). Importantly, given that lamellipodial extension increases the HGF responsiveness and that subsequent sustained Met-ERK activation in turn promotes the lamellipodial protrusion, these two events constitute a positive feedback loop (Figure S7). This positive feedback loop would be responsible for the leader cell specification at the free edge. Although FA formation is more prominent in the leader cells than the follower cells, the FA formation does not require HGF signaling (Figure 6B). Thus, immature focal complex is prerequisite for the lamellipodial protrusion and ERK activation, but mature FAs are not directly involved in the positive feedback loop. Also, the coupling of the signal activation with lamellipodial extension would be beneficial for the downregulation of the leader cells after the free space is closed by the migrating cells. Collectively, the results of the present study identified that physical environment and biochemical cues cooperatively regulate the leader cell specification during the collective migration of epithelial cells.

We have demonstrated that the lamellipodial protrusion endows HGF sensitivity, but the detailed mechanism still remains unclear. A clue observation might be the effect of surfen, which is known to prevent the binding of growth factors to HSPGs (Figures S6F and S6G). Surfen blocks the HGF-induced sustained ERK activation, suggesting that HSPGs function to

enhance HGF-Met signaling exclusively in the leader cells. If so, why do HSPGs function only in the leader cells? Although this is still an open question awaiting future investigation, it is known that some HSPGs, including glypican family proteins, glycosylphosphatidylinositol (GPI)-anchored proteins (Li et al., 2018), and syndecan (Morgan et al., 2007) have been shown to enhance cellular sensitivity to FGF and VEGF as well as HGF (Derksen et al., 2002; Elfenbein et al., 2012; Jakobsson et al., 2006; Ornitz, 2000). Interestingly, a recent study has shown that integrin-mediated cell spreading promotes the clustering of GPI-anchored proteins (Kalappurakkal et al., 2019). Also, lamellipodial protrusions are proposed to be enriched with lipid rafts (Kim et al., 2011; Manes et al., 1999) and some HSPGs are potentially localized to the lipid rafts (Chu et al., 2004; Gutierrez et al., 2014). Therefore, future studies will explore the role of HSPGs localized in lipid rafts in the clustering of HGF-Met complex, presumably important for the HGF-dependent ERK activity in leader cells.

We also found that Arp2/3-mediated lamellipodial extension is required for the HGF-dependent ERK activation in the leader cells (Figure 5). Besides the above-mentioned mechanism mediated by lipid rafts, the actin polymerization may directly promote receptor tyrosine kinase dimerization. A previous report has shown that EGFR dimerization and EGF-EGFR binding preferentially occur at the cell periphery in an actin polymerization-dependent manner (Chung et al., 2010). Additionally, it is known that cell protrusion increases the sensitivity of cells to EGF in a focal adhesion kinase (FAK)-dependent manner (Yang et al., 2018). We speculate that similar mechanism(s) might also regulate the HGF-Met activation.

Our results revealed that talin1-mediated cell-substrate contacts are prerequisite for the HGF sensitivity (Figure 6). Previous studies have shown that the HGF sensitivity is negatively regulated by cell density (Machide et al., 2006; Mizuno et al., 1993). Yet, how cells sense the surrounding environment for the density-dependent HGF sensitivity was unclear despite the implication of integrin expression in the regulation of HGF sensitivity (Ephstein et al., 2013; Liu et al., 2009). In the present study, free space-dependent lamellipodial protrusions, but not adherens junctions, function to sense the emergence of free edge, thereby enhancing the HGF sensitivity. The free edge-dependent regulation is critical for the spatial patterning of leader cell specification during collective cell migration. We expect that this mechanism would also provide insight into the long-standing mystery of the injured organ-specific HGF sensitivity (Nakamura and Mizuno, 2010).

In the leader cells, ERK activation promotes lamellipodial extension (Figure 7). This is in stark contrast to the confluent cells, where ERK activation triggers cell contraction (Hino et al., 2020). What engenders these opposite outcomes after the ERK activation? We speculate that the outcomes of ERK activation would depend on the presence of cell-cell junctions. During collective cell migration, Rho-associated kinase (ROCK) is activated in confluent cells in an ERK-dependent manner (Hino et al., 2020). ROCK increases phosphorylation of myosin through direct phosphorylation and inhibition of myosin phosphatase (Amano et al., 1996; Kimura et al., 1996; Totsukawa et al., 2000), thereby inducing cell contraction. Importantly, in confluent cells, ROCK also functions to suppress Rac1 by recruiting FilGAP/ARHGAP24, a Rac GTPase-activating protein (GAP) to cell-cell junctions (Nakahara et al., 2015). Moreover, at cell-cell junctions, Rac1 activity is also suppressed through the Merlin-Angiomotin-Rich1 axis (Das et al., 2015; Yi et al., 2011) and through cingulin and

paracingulin-mediated recruitment of MgcRacGAP/RACGAP1 (Guillemot et al., 2014). These mechanisms presumably suppress ERK-mediated lamellipodial extension specifically in follower cells by inhibiting Rac1 at the cell-cell junctions during collective migration. In fact, the lamellipodia in follower cells, known as cryptic lamellipodia, is less prominent, if any, compared with that in leader cells (Farooqui and Fenteany, 2005). Meanwhile, at the free edge of the leader cells, Rac1 may be liberated from the cell-cell junction-mediated inhibition, resulting in the generation of large lamellipodial protrusions. Note that optogenetic sustained ERK activation in confluent cells causes cell contraction (Hino et al., 2020); whereas that in leader cells causes lamellipodial protrusion (Figure 7A), highlighting the effect of cell-cell junction on the outcomes of ERK activation. Thus, we assume that the Rac1 suppression by cell-cell junctions would serve as a safeguard mechanism, ensuring that only cells devoid of cell-cell junctions exhibit leader cell properties upon HGF-Met-ERK activation.

Cooperativity between mechanical and biochemical cues has been proposed to be the critical process in the regulation of tissue development and regeneration (Hannezo and Heisenberg, 2019). Collective cell migration in various tissues is also regulated by growth factors (Chmielowiec et al., 2007; Duchek and Rorth, 2001; Durdu et al., 2014; Gerhardt et al., 2003; McDonald et al., 2003) and mechanical cues (Barriga et al., 2018; Cai et al., 2014). Our findings will shed light on the feedback loop between physical environment and biochemical cues that underlies leader cell specification during the collective cell migration not only of epithelial cells, but also of other systems during tissue development.

Limitations of the Study

Our analysis on the role of endocytosis is limited to the usage of an endocytosis inhibitor dynasore. Alternative approaches are required for systematically determining the role of endocytosis in the regulation of HGF-dependent ERK activation in leader cells. Additionally, the detailed mechanisms of lamellipodia-dependent HGF-Met-ERK activation needs to be further addressed in the future studies.

Acknowledgements

We thank the members of the Matsuda Laboratory for their helpful discussion and encouragement, and K. Hirano and K. Takakura for their technical assistance. This work was supported by the Kyoto University Live Imaging Center. Financial support was provided in the form of JSPS KAKENHI grants (nos. 17J02107 and 20K22653 to N. Hino, and 20H05898 and 19H00993 to M. Matsuda), a JST CREST grant (no. JPMJCR1654 to M. Matsuda), a Moonshot R&D grant (no. JPMJPS2022-11 to M. Matsuda), Generalitat de Catalunya and the CERCA Programme (no. SGR-2017-01602 to X. Trepat), MICCINN/FEDER (no. PGC2018-099645-B-I00 to X. Trepat), and European Research Council (no. Adv-883739 to X. Trepat). IBEC is a recipient of a Severo Ochoa Award of Excellence from the MINECO. This work was partly supported by Extramural Collaborative Research Grant of Cancer Research Institute, Kanazawa University.

Author contributions

Conceptualization, N.H., M.M.; Methodology, N.H., K.T., T.H., M.M.; Software, N.H., T.X., K.M.; Validation, N.H., K.M., Y.J., M.M.; Formal analysis, N.H., K.M.; Investigation, N.H., K.M.; Resources, N.H., K.M., G.M., K.S., R.I., S.T., K.A., K.T., T.H., X.T., M.M.; Data curation, N.H., K.M., M.M.; Writing - original draft, N.H., M.M.; Writing - review & editing, N.H., M.M.; Visualization, N.H., K.M., M.M.; Supervision, N.H., M.M.; Project administration, N.H., M.M.; Funding acquisition, N.H., K.T., X.T., M.M.

Declaration of interests

The authors declare no competing interests.

Main figure titles and legends

Figure 1. Leader cells show sustained ERK activation independently of EGFR activity

(A) Schematics of the confinement release assay. MDCK cells expressing EKARrEV-NLS were cultured within a culture insert. After removal of the culture insert, the cells facing the free space migrated as leader cells.
(B) Cells in Medium 199 containing 10% FBS were observed every 5 min up to 24 hr under fluorescence microscopes. Differential interference contrast (DIC) images (left), FRET/CFP ratio images representing ERK activity (center), and magnified images of the regions indicated by broken lines (right) are represented at 0, 5, 10, and 15 hr. Scale bar, 200 μm.
(C) A kymograph of the ERK activity shown in (B).
(D) Heatmaps of ERK activity in the 21 leader and 21 follower cell regions Each row of the heatmaps represents a single region.
(E) Mean ERK activities in the follower and the leader cell regions from 4.5 to 19 hr after the start of the imaging. The red bars represent the means and SDs. Welch's t-test, n = 21 from three independent experiments.
(F) Kymographs of ERK activity before and after the addition of 0.1% DMSO (upper) or 2 μM PD153035 (EGFR inhibitor; lower). The imaging interval was 5 min. Broken lines represent the timing of drug treatment.
(G) Heatmaps of ERK activity in the follower (left) and leader (right) cell regions before and after 0.1% DMSO (upper) and 2 μM PD153035 (EGFR inhibitor; lower) treatment. Twenty-one regions were analyzed for each condition.
(H) ERK activities in the leader and the follower cell regions 3 hr after the drug treatment are represented as dots. The red bars indicate the means and SDs. Dunnett's T3 multiple comparisons test, n = 21 from three independent experiments.
See also Figure S1 and S2; Video S1 and S2.

Figure 2. HGF triggers sustained ERK activation in leader cells

(A) MDCK cells expressing EKARrEV-NLS were subjected to the confinement release assay. ERK activity images of cells cultured with (left) and without (right) 10% FBS are represented at 0.5 before (upper) and 3 hr after (right) the addition of 2 μM PD153035 (EGFR inhibitor).

(B) Heatmaps of ERK activity in the 21 leader cell regions with (left) and without (right) 10% FBS before and after 2 μM PD153035 addition. The imaging interval was 5 min.
(C) ERK activities in the leader cell regions 3 hr after the drug treatment are represented as dots. The red bars indicate the means and SDs. Welch's t-test, n = 21 from three independent experiments.
(D) Images of ERK activity in serum-free media containing 2 μM PD153035. Cells were unstimulated (left) or stimulated with 2.5 ng mL^{-1} HGF treatment (right).
(E and F) Kymographs of the ERK activity shown in (D). The imaging interval was 5 min.
(G) ERK activities in the leader cells 2 hr after the HGF treatment are represented as dots. The red bars indicate the means and SDs. Dunnett's T3 multiple comparisons test, n = 39 cells (follower, HGF (−)), 54 cells (follower, HGF (+)), 33 cells (leader, HGF (−)), and 33 cells (leader, HGF (+)) from three independent experiments.
(H) Images of ERK activity in WT and Met KO clone #1 cells cultured in FBS-containing media are represented at −0.5 (upper) and 2 hr (lower) after 2 μM PD153035 (EGFR inhibitor) treatment. The imaging interval was 5 min.
(I and J) Kymographs of the ERK activity shown in (H).
(K) ERK activities in the leader cells 2 hr after the EGFR inhibitor treatment are represented as dots. The red bars indicate the means and SDs. Dunnett's T3 multiple comparisons test, n = 33 cells (WT), 33 cells (Met KO clone #1), and 37 cells (Met KO clone #2) from three independent experiments.
(L) Schematics of an *in vivo* imaging of ERK activity during wound healing of mouse ear skin expressing hyBRET-ERK-NES.
(M) ERK activity images of mouse ear skin are represented at 0, 0.5, 2, 2.5 hr after the start of the imaging. Mice were treated with 100 mg kg^{-1} erlotinib (EGFR inhibitor) and 10 mg kg^{-1} glumetinib (Met inhibitor) administered by intraperitoneal injections at 0 and 2 hr, respectively. The broken lines indicate wound edges. The yellow arrowheads indicate leader cells.
(N) ERK activities in the leader and follower cells in (M). Each line represents different positions. Dunn's multiple comparisons test, n = 6 positions from three independent experiments using 3 mice.
See also Figure S1 and S2; Video S3 and S4.

Figure 3. The HGF-Met signaling pathway is activated primarily in the leader cells despite similar Met expression level to the follower cells

(A) MDCK cells were subjected to confinement release assay in the FBS-free medium containing 2.5 ng mL^{-1} HGF. The cells were fixed 6 hr after the start of migration. Fluorescence images of Met immunofluorescence and nuclei (CFP of EKARrEV-NLS) are shown. The upper image indicates the Met signal intensity, and the lower image shows the merged image of Met (green) and nucleus (blue).
(B) Mean values of Met intensity binned every 50 μm from the leader cells are plotted over the distance from the leader cells, with SDs. Dunnett's T3 multiple comparisons test, n > 25 from three independent experiments.

(C) MDCK cells were subjected to confinement release assay in the FBS-free medium containing 2.5 ng mL^{-1} HGF, and were treated with 2 μM PD153035 3 hr after the start of migration. The cells were fixed 6 hr after the start of migration and subjected to immunofluorescence by using anti-Met antibody without permeabilization. xy (upper) and xz (middle) sections of the z-stack fluorescence images of Met immunofluorescence are shown. Magnified images (lower) of the follower and leader cells indicated by black lines below the xz section image (middle) are represented.
(D) MDCK cells expressing miRFP670-HRasCT (red) and EKARrEV-NLS (blue) were subjected to the confinement release assay in the FBS-free medium containing 2 μM PD153035. Rhodamine-HGF (green) were applied at time 0. The maximum projection image (upper), segmented cell image (middle), and ERK activity image (bottom) at 5.5 hr after the Rhodamine-HGF treatment are shown. The segmented cells are color-coded according to their cell area.
(E–G) Mean values of Rhodamine-HGF intensity (E), cell area (F), and ERK activity (G) binned every 50 μm from the leader cells 5.5 hr after the HGF treatment are plotted over the distance from the leader cells, with SDs. The data were pooled from three independent experiments.
(H and I) Scatter plots of Rhodamine-HGF intensity (H) and cell area (I) versus ERK activity. Each dot represents a single cell and is color-coded according to the distance from the leader cells. Spearman's correlation *r*, n = 1,449 from three independent experiments.
(J–L) MDCK cells expressing miRFP670-HRasCT (red) and EKARrEV-NLS (blue) were subjected to the confinement release assay in the FBS-free media containing 2 μM PD153035 as well as 0.1% DMSO, 80 μM Dynasore (endocytosis inhibitor), or 1 μM glumetinib (Met inhibitor). Rhodamine-HGF (green) were applied 2 hr after the start of migration. (J) The maximum projection images of the cells cultured in the media containing DMSO (left), endocytosis inhibitor (center), or Met inhibitor (right) at 5.5 hr after the Rhodamine-HGF treatment are shown. (K) Mean values of Rhodamine-HGF intensity in the cells treated with DMSO (orange), endocytosis inhibitor (blue), or Met inhibitor (green) binned every 50 μm from the leader cells at 5.5 hr after the HGF treatment are plotted over the distance from the leader cells, with SDs. The data were pooled from three independent experiments. (L) ERK activities in the leader cells located within 50 μm from the leading edge are represented as dots. The red bars indicate the means and SDs. Dunnett's T3 multiple comparisons test, n = 21 cells (DMSO), 20 cells (endocytosis inhibitor), and 23 cells (Met inhibitor) from three independent experiments.
See also Figure S3 and S4.

Figure 4. HGF activates Ras at the lamellipodia of leader cells

(A) MDCK cells expressing Raichu-454HRasCT, a FRET biosensor for Ras activity, were subjected to the confinement release assay in FBS-free medium containing 2 μM PD153035 without (upper) or with (lower) 2.5 ng mL^{-1} HGF. Images of the follower (left) and the leader (right) cells are shown.

(B) Ras activities in the follower and the leader cells 3 hr after the start of the imaging are represented as dots. The red bars indicate the means and SDs. Welch's t-test, n = 99 cells (follower, HGF (−)), 26 cells (leader, HGF (−)), 58 cells (follower, HGF (+)), and 13 cells (leader, HGF (+)) from at least three independent experiments.
(C) Each cell was divided into two regions at the center of mass of the cell to define the cell front and rear, and the two regions were measured for Ras activity. The red bars indicate the means and SDs. Welch's t-test, n = 58 cells (follower) and 13 cells (leader) from at least three independent experiments.
See also Video S5.

Figure 5. Lamellipodial extension after the release from mechanical confinement increases the HGF sensitivity of leader cells

(A–D) Wild type MDCK cells and α-1-catenin knock-out (KO) MDCK cells expressing EKARrEV-NLS were subjected to confinement release assay in the FBS-free medium containing 2.5 ng mL^{-1} HGF. (A) Images 0.5 hr before (upper) and 2 hr after (lower) 2 μM PD153035 addition are shown. (B and C) Kymographs of the ERK activity shown in panel (A). The imaging interval was 5 min. (D) ERK activities in the follower and the leader cells 2 hr after the EGFR inhibitor treatment are represented as dots. Welch's t-test, n = 54 cells (WT, follower), 33 cells (WT, leader), 33 cells (α-1-catenin KO clone #1, follower), 33 cells (α-1-catenin KO clone #1, leader), 39 cells (α-1-catenin KO clone #2, follower), and 33 cells (α-1-catenin KO clone #2, leader) from three independent experiments.
(E and F) Cells cultured in the FBS-free media containing 2.5 ng mL^{-1} HGF with (left) or without confinement (right) were treated with 2 μM PD153035 3.5 hr after the start of imaging. (E) Images 2 hr after 2 μM PD153035 addition are shown. The blue broken lines represent the outline of the confinement. (F) ERK activities in the cells at the periphery of the epithelial cell sheet 2 hr after the EGFR inhibitor treatment are represented as dots. Welch's t-test, n = 33 from three independent experiments.
(G and H) MDCK cells expressing EKARrEV-NLS were subjected to confinement release assay in the FBS-free media containing 2.5 ng mL^{-1} HGF and 2 μM PD153035. Cells were treated with 0.1% DMSO (left), 100 μM CK666 (Arp2/3 inhibitor; center), and 1 μM Latrunculin A (right) 3.5 hr after the start of imaging. (G) Images 2 hr after the drug treatment are shown. (H) ERK activities in the leader cells 2 hr after the drug treatment are represented as dots. Dunnett's T3 multiple comparisons test, n = 33 from three independent experiments.
(I–K) MDCK cells expressing EKARrEV-NLS, mCherry-HRasCT, and miRFP703-^{iK6}DHFR-Tiam1(DH-PH) were co-cultured with MDCK cells without these genes, and subjected to confinement release assay in the FBS-free medium containing 2 μM PD153035 with (right) or without 2.5 ng mL^{-1} HGF (left). Cells were treated with 0.1% DMSO or 10 μM m^{D}cTMP 1 hr after the start of imaging. (I) ERK activity images of the follower cells are represented at immediately before (left) and 20 min after (right) the addition of 10 μM m^{D}cTMP. The white arrow heads indicate cells expressing the SLIPT system. The yellow arrow heads show lamellipodial protrusions induced by the m^{D}cTMP treatment. (J) Schematics of the SLIPT system. (K) ERK activities in the follower cells were plotted as a function of time after the

drug treatment with 0.1% DMSO (blue) or 10 μM m^DcTMP (orange). The lines represent mean ± SDs. n = 21 cells (HGF(−), DMSO), 27 cells (HGF(−), m^DcTMP), 21 cells (HGF(+), DMSO), 38 cells (HGF(+), m^DcTMP) from three independent experiments.
See also Figure S5; Video S6 and S7.

Figure 6. Talin1-mediated immature focal complex is required for the HGF-dependent sustained ERK activation

(A–E) MDCK cells were subjected to a confinement release assay in the FBS-free medium. (A) The cells were treated with 2 μM PD153035 at 3 hr after the start of migration in the absence (left) or presence (right) of 2.5 ng mL^{-1} HGF. Cells were immunostained with anti-paxillin (upper) and anti-pERK (lower) antibodies. The middle images are magnified images of the regions corresponding to the numbered windows in the upper images. (B and C) Mean values of paxillin-positive FA intensity (B) and pERK intensity (C) binned every 50 μm from the free edge 6 hr after the start of migration are plotted over the distance from the leader cells, with SDs. The data were pooled from three independent experiments. (D and E) Scatter plots of paxillin-positive FA intensity versus pERK mean intensity in the absence (D) or presence (E) of HGF. Each dot represents a single cell and is color-coded according to the distance from the leader cells. Spearman's correlation *r*, n = 404 cells (D) and n = 357 cells (E) from three independent experiments.
(F and G) Wild type and talin1 KO MDCK cells expressing EKARrEV-NLS were subjected to confinement release assay in FBS-free medium containing 2.5 ng mL^{-1} HGF. (F) Images 0.5 hr before (upper) and 1.5 hr after (lower) 2 μM PD153035 addition are shown. The imaging interval was 5 min. (G) ERK activities in the leader cells 1.5 hr after the EGFR inhibitor treatment are represented as dots. Dunnett's T3 multiple comparisons test, n = 33 cells from three independent experiments.
(H and I) MDCK cells expressing EKARrEV-NLS were subjected to confinement release assay in FBS-free medium containing 2.5 ng mL^{-1} HGF and 2 μM PD153035. (F) Images 0.5 hr before (upper) and 2 hr after (lower) 0.1% DMSO (left) or 30 μM Y-27632 (ROCK inhibitor, right) addition are shown. The imaging interval was 5 min. (I) ERK activities in the leader cells 2 hr after the EGFR inhibitor treatment are represented as dots. Welch’s t-test, n = 33 cells from three independent experiments.
See also Figure S6; Video S8.

Figure 7. ERK activation in leader cells triggers lamellipodial protrusion of the leader cells and increases traction force

(A and B) MDCK cells expressing 2paRAF composed of membrane-targeted CIBN-mScarlet-I and BFP-CRY2-Raf1 were subjected to the confinement release assay in FBS-free media containing 2.5 ng mL^{-1} HGF and 2 μM PD153035, and 0.1% DMSO (left), 200 nM trametinib (MEK inhibitor, center), or 100 μM CK666 (Arp2/3 inhibitor, right). (A) Images before and 2 hr after photoactivation of Raf1 are shown. The blue and yellow dotted lines outline representative cells. (B) Changes in cell area are plotted over time after blue light exposure.

Each line indicates the cell area change of a corresponding leader cell. The red lines indicate the mean values. Dunnett's T3 multiple comparisons test, n = 27 cells (DMSO), 24 cells (MEK inhibitor), and 26 cells (Arp2/3 inhibitor) from three independent experiments. (C–E) Traction force microscopy of cells cultured in media containing 2 μM PD153035 without (left) and with (right) 2.5 ng mL^{-1} HGF on 3 kPa polyacrylamide gels. (C) Traction force along the x-axis (upper) and along the y-axis (middle) as well as DIC images (lower) are represented at 0 and 3.5 hr after the start of the imaging. (D and E) Mean traction force along the x-axis (D) and y-axis (E) under the leader cells at 3.5 hr after the start of the imaging is plotted. Welch's t-test, n = 27 from three independent experiments.
See also Video S9.

STAR Methods text

RESOURCE AVAILABILITY

Lead Contact

Further information and requests for resources and reagents should be directed to and will be fulfilled by the Lead Contact, Naoya Hino (naoya.hino@ist.ac.at).

Materials Availability

- Plasmids generated in this study have been deposited to Addgene. The plasmid numbers are listed in the key resource table.
- Cell lines established in this study have been deposited to Japanese Collection of Research Bioresources (JCRB) Cell Bank. The identifiers are listed in the key resource table.

Data and Code Availability

- Microscopy data and original immunoblot images collected for this study have been deposited to Systems Science of Biological Dynamics repository (SSBD:repository) and are publicly available as of the date of publication. DOI is listed in the key resource table.
- Any additional information required to reanalyze the data reported in this paper is available from the lead contact upon request.
- This study does not report original code.

EXPERIMENTAL MODEL AND SUBJECT DETAILS

Cell culture

MDCK and Lenti-X 293T cells were provided from RIKEN BioResource Center (no. RCB0995) and Clontech (no. 632180; Mountain View, CA), respectively. These cells were cultured in D-MEM (no. 044-29765; Wako, Osaka, Japan) supplemented with 10% FBS (F7524; Sigma), 100 units mL^{-1} penicillin, and 100 μg mL^{-1} streptomycin (no. 26253-84; Nacalai Tesque, Kyoto, Japan) in a 5% CO2 humidified incubator at 37°C.

Establishment of stable cell lines

A lentiviral expression system was employed to establish MDCK cells stably expressing EKARrEV-NLS as described previously (Hino et al., 2020; Lin et al., 2022). Briefly, for the preparation of the lentivirus, pCSII-EKARrEV-NLS (Lin et al., 2022), a vector for lentiviral transduction (Miyoshi et al., 1998), psPAX2 (Addgene Plasmid: no. 12260), and pCMV-VSV-G-RSV-Rev were co-transfected into Lenti-X 293T cells by using polyethylenimine (no. 24765-1; Polyscience Inc., Warrington, PA). MDCK cells were incubated with the lentivirus and after 2 days of incubation the cells were treated with 10 μg mL^{-1} blasticidin S (no. 029-18701; Wako, Okasa, Japan) for the selection. The obtained MDCK cells were subjected to single-cell cloning to achieve a uniform expression level of the biosensor. MDCK cells stably expressing Raichu-Ras with an H-Ras membrane-targeting sequence (HRasCT: KLNPPDESGPGCMSCKCVLS), miRFP670-HRasCT, mCherry-HRasCT, or miRFP703-^{iK6}DHFR-Tiam1 (DH-PH) were established with a piggyBac transposon system. pPB plasmids (pPBbsr2-Raichu-454HRasCT, pPBpuro-miRFP670-HRasCT, pPBpuro-mCherry-HRasCT, or pPBbleo-miRFP703-^{iK6}DHFR-Tiam1(DH-PH)) and pCMV-mPBase(neo-) encoding *piggyBac* transposase were co-transfected into MDCK cells by electroporation with an Amaxa nucleofector (Lonza, Basel, Switzerland), followed by selection with appropriate antibiotics (10 μg mL^{-1} blasticidin S. for bsr, 4 μg mL^{-1} puromycin (no. P-8833, SIGMA) for puro, or 100 μg mL^{-1} zeocin (no. R250-05, Thermo Fisher Scientific) for bleo). After the selection, the Raichu-454HRasCT-expressing cells were subjected to single-cell cloning. The cells expressing miRFP670-HRasCT or mChery-HRasCT/miRFP703-^{iK6}DHFR-Tiam1 (DH-PH) were sorted by FACS to obtain the cells with high expression level. To establish MDCK cells stably expressing 2paRAF (Kinjo et al., 2019), pT2ADWpuro_2paRAF was introduced into cells by using the Tol2 transposon system as described previously (Hino et al., 2020). Briefly, MDCK cells were co-transfected with pT2ADWpuro_2paRAF and pCAGGS-T2TP encoding Tol2 transposase by electroporation, followed by selection with 4 μg mL^{-1} puromycin.

CRISPR/Cas9-mediated KO cell lines

For CRISPR/Cas9-mediated KO of dog Met (*MET*) and α-1-catenin (*CTNNA1*), single guide RNAs (sgRNA) targeting the exons were designed using CRISPRdirect (Naito et al., 2015). The sgRNAs were designed as follows: α-catenin sgRNA, GTAGAAGATGTTCGAAAACA; Met sgRNA, TGGGTGGAAGGATATGTCGC. Oligo DNAs for the sgRNA were cloned into the PX459 vectors, and the vectors were transfected into MDCK cells by electroporation. The transfected cells were treated with 4.0 μg mL^{-1} puromycin for selection. After the selection and subsequent single-cell cloning, the KO of the protein of interest in each clone was checked by immunoblotting. For CRISPR/Cas9-mediated KO of dog talin1 (*TLN1*), single guide RNAs targeting the exon and adjacent intron were designed and incorporated into the PX459 vectors, respectively. The two following sequences were used for the sgRNAs: talin1 sgRNA targeting an exon: TTCCATCAGCTCTCGAACCA; talin1 sgRNA targeting an intron: GGGTGGGGGCAACTGTTGAT. Two PX459 vectors which include the above-mentioned sgRNAs were simultaneously transfected into MDCK cells by electroporation,

741 followed by selection with 4.0 μg mL^{-1} puromycin and subsequent single-cell cloning to
742 obtain talin1 KO cells. Two clones (clone #1 and #2) were obtained for each KO procedure.
743
744 **METHOD DETAILS**

745 **Reagents and antibodies**
746 The following reagents were used: trametinib (no. T-8123; LC Laboratories, Woburn, MA),
747 PD153035 hydrochloride (no. SML0564-5MG; SIGMA, St. Louis, MO), CK666 (no.
748 SML0006-5MG; SIGMA), latrunculin A (no. 125-04363; Wako, Osaka, Japan), erlotinib
749 hydrochloride (no. 057-09111; Wako), glumetinib (no. HY-116000; MedChemExpress,
750 Monmouth Junction, NJ), Dynasore (no. sc-202592; Santa Cruz Biotechnology, Dallas, TX),
751 Y-27632 (no. 253-00513, Wako), and human recombinant HGF (no. 4509-10; BioVision,
752 Milpitas, CA).
753 The following primary and secondary antibodies were used for immunoblotting: anti-
754 phospho-Met (Tyr1234/1235) rabbit antibody (no. 3077S; Cell Signaling Technology, 1:1,000
755 dilution); anti-phospho-RAF1 (Ser338) rabbit antibody (no. 9427; Cell Signaling Technology,
756 1:1,000 dilution); anti-ERK1/2 mouse antibody (no. 610123; BD Biosciences, 1:2,000
757 dilution); anti-phospho-p44/42 MAPK (Erk1/2; Thr202/Tyr204) rabbit antibody (no. 4370;
758 Cell Signaling Technology, 1:1,000 dilution); IRDye 680-conjugated goat anti-mouse IgG
759 antibody (no. 926-32220; LI-COR Biosciences, Lincoln, NE, 1:10,000 dilution); and IRDye
760 800CW goat anti-rabbit IgG antibody (no. 926-32211; LI-COR Biosciences, 1:10,000
761 dilution).
762 The following primary and secondary antibodies were used for immunofluorescence:
763 anti-phospho-p44/42 MAPK (Erk1/2; Thr202/Tyr204) rabbit antibody (no. 4370; Cell
764 Signaling Technology, 1:100 dilution); anti-paxillin mouse antibody (no. 03-6100; ZYMED,
765 1:100 dilution); anti-canine Met goat antibody (no. AF4140; R&D systems, Minneapolis,
766 MN, 1:100 dilution); anti-EGF Receptor rabbit antibody (no. 4267, Cell Signaling
767 Technology, 1:100 dilution); alexa 647-conjugated goat anti-mouse IgG (H+L) antibody (no.
768 A-21235; Thermo Fisher Scientific, Waltham, MA, 1:1,000 dilution); alexa 647-conjugated
769 goat anti-rabbit IgG (H+L) antibody (no. A-21245; Thermo Fisher Scientific, 1:1,000
770 dilution); alexa 568-conjugated goat anti-rabbit IgG (H+L) antibody (no. A-11036; Thermo
771 Fisher Scientific, 1:1,000 dilution); and alexa 568-conjugated donky anti-goat IgG (H+L)
772 antibody (no. A-11057; Thermo Fisher Scientific, 1:1,000 dilution).
773
774 **Confinement release assay**
775 To observe collectively migrating MDCK cells, a confinement release assay was performed as
776 described previously with slight modification (Hino et al., 2020). MDCK cells were
777 confluently seeded into a 2-well culture insert (no. 81176; ibidi, Martinsried, Germany; $9.8 \times$
778 10^3 cells in each well) placed on a glass-bottom dish coated with 0.3 mg mL^{-1} type I collagen
779 (Nitta Gelatin, Osaka, Japan). After 20 hr of incubation, the cells were released for migration
780 by removing the culture insert and changing the medium to Medium 199 (11043023; Life
781 Technologies, Carlsbad, CA) supplemented with 100 units mL^{-1} penicillin, 100 μg mL^{-1}

streptomycin, and 1% bovine serum albumin (BSA) (no. A2153-50G; SIGMA) or 10% fetal bovine serum (FBS) with or without additional chemicals as indicated in the figure legends.

Time-lapse imaging of MDCK cells

Images of MDCK cells were collected and processed with basically the same conditions and procedures as previously described (Aoki and Matsuda, 2009). Briefly, for FRET imaging and the experiments of optogenetics, cells were observed with IX81 and IX83 inverted microscopes (Olympus, Tokyo, Japan), respectively. The IX81 inverted microscope was equipped with a UPlanAPO 10x/0.40 (Olympus), a UPlanSAPO 20x/0.75 (Olympus), or a UPlanSAPO 40x/0.95 objective lens (Olympus), a QI-695 CCD camera (Molecular Devices, Sunnyvale, CA), a CoolLED precisExcite light-emitting diode (LED) illumination system (Molecular Devices), an IX2-ZDC laser-based autofocusing system (Olympus), an MD-WELL96100T-Meta automatically programmable XY stage (Sigma Koki, Tokyo, Japan), and a stage top incubator (Tokai Hit, Fujinomiya, Japan). The filters and dichromatic mirrors used for time-lapse imaging with the IX81 microscope were as follows: for FRET imaging, an FF02-438/24-25 excitation filter (Semrock, Rochester, NY), an FF458-Di02-25x36 (Semrock) dichromatic mirror, and an FF01-483/32-25 (Semrock) and FF01-542/27-25 (Semrock) emission filter for CFP and FRET, respectively. For mCherry imaging, a 560DF15 excitation filter (Omega Optical, Brattleboro, VT), a U-MWIGA3 dichromatic mirror (Olympus), and an FF01-624/40-25 (Semrock) emission filter were used. The IX83 microscope was equipped with a UPlanSAPO 20x/0.70 (Olympus), a Prime sCMOS camera (Photometrics, Tucson, AZ), a CoolLED precisExcite light-emitting diode (LED) illumination system (Molecular Devices), an IX3-ZDC laser-based autofocusing system (Olympus), an MD-WELL96100T-Meta automatically programmable XY stage (Sigma Koki), and a stage top incubator (Tokai Hit). The filters and dichromatic mirrors used for time-lapse imaging with the IX83 inverted microscope were as follows: for FRET imaging, an ET430/24x excitation filter (Chroma Technology, Bellows Falls, VT), an XF2034 (455DRLP) dichromatic mirror (Omega Optical), and an FF01-483/32-25 (Semrock) and an ET535/30m emission filter (Chroma Technology) for CFP and FRET, respectively. For mScarlet-I imaging, a ET572/35x excitation filter (Chroma Technology), an 89006 dichromatic mirror (Chroma Technology), and an ET632/60m (Chroma Technology) emission filter were used.

For the SLIPT experiment, cells were observed with a Ti2 inverted microscope (Nikon, Tokyo, Japan). The Ti2 inverted microscope was equipped with a Plan Fluor DIC 40x/0.75 (Nikon), an ORCA-Fusion C1440-20UP CMOS camera (HAMAMATSU PHOTONICS, Hamamatsu, Japan), X-Cite TURBO (Excelitas Technologies, Waltham, MA), and a stage top incubator (Tokai Hit). The filters and dichromatic mirrors used for time-lapse imaging with the Ti2 microscope were as follows: For FRET imaging, an 434/32 excitation filter (Nikon), a 425 dichromatic mirror (Nikon), and 480/40 and 535/30 emission filters (Nikon) for CFP and FRET, respectively, were used. For mCherry imaging, a 570/40 excitation filter (Nikon), a 600 dichromatic mirror (Nikon), and a 645/75 emission filter (Nikon) were used. For miRFP703 imaging, a 640/14 excitation filter (Nikon), a 660 dichromatic mirror (Nikon), and a 700/75 emission filter (Nikon) were used.

In vivo two-photon imaging of wound healing

The establishment of mice stably expressing hyBRET-ERK-NES and the *in vivo* imaging procedures were described previously (Hiratsuka et al., 2015; Komatsu et al., 2018). Briefly, 8- to 20-week-old female mice were used for the *in vivo* imaging. The animal protocols were approved by the Animal Care and Use Committee of Kyoto University Graduate School of Medicine (approval nos. 19090, 20081). The experiments were carried out under the relevant regulations. Eighteen hours before the start of the imaging, mice were anesthetized with 1.5% isoflurane (Abbot Japan, Tokyo, Japan), the ear hair was removed, and a surgical scalpel was used to create shallow epithelial wounds on the ear skin with as little damage to the dermis as possible. The mice were then imaged under a 2P excitation inverted microscope (FV1200MPE; Olympus). The interval of the z-stack imaging was set at 1 μm. During the imaging, mice were treated with erlotinib 100 mg kg^{-1} and glumetinib 10 mg kg^{-1} by intraperitoneal injections at the time points indicated in the figures. For the quantification of the data, leader and follower cell regions (about 50 μm distant from the wound edge) were manually defined, and the FRET/CFP ratio was obtained from the regions.

The FV1200MPE inverted microscope was equipped with a UPLSAPO30XS lens (Olympus), and an InSight DeepSee Ultrafast laser (Spectra Physics, Mountain View, CA). An infrared light-cut filter, RDM690 (Olympus); two dichromatic mirrors, DM505 and DM570 (Olympus); and two emission filters, BA460-500 (Olympus) for CFP and BA520-560 (Olympus) for FRET, were used.

Analysis of HGF signaling by immunoblotting

MDCK cells were seeded on collagen-coated 48-well (confluent condition: 4.4×10^4 cell cm^{-2}) and 6-well plates (sparse condition: 4.1×10^3 cell cm^{-2}). After 20 hr of incubation, the media were replaced with Medium 199 with 100 units mL^{-1} penicillin, 100 μg mL^{-1} streptomycin, and 1% BSA with 1 μM PD153035 (EGFR inhibitor) to suppress EGFR-dependent ERK activation. After further incubation for 1.5 hr, a final 2.5 ng mL^{-1} HGF was added to the media. The cells were lysed with SDS sample buffer containing 62.5 mM Tris-HCl (pH 6.8), 12% glycerol, 2% SDS, 40 ng mL^{-1} bromophenol blue, and 5% 2-mercaptoethanol, sonicated with a Bioruptor UCD-200 (Cosmo Bio, Tokyo, Japan), and then boiled at 95°C for 5 min. The samples were resolved by SDS-PAGE with SuperSep Ace 5-20% precast gels (Wako), and transferred to PVDF membranes (Merck Millipore, Billerica, MA). All primary antibodies were diluted in Odyssey blocking buffer (LI-COR Biosciences). For detection of phospho-Met and phospho-/pan-ERK, secondary antibodies were diluted in Odyssey blocking buffer containing 0.01% SDS. For detection of phospho-Raf1, secondary antibodies were diluted in Odyssey blocking buffer without supplementation of SDS. Fluorescent signals were detected by an Odyssey Infrared Imaging System (LI-COR Biosciences).

Cell density-dependent ERK activation

MDCK cells were seeded into a culture insert placed on a glass-bottom dish coated with 0.3 mg mL^{-1} type I collagen (confluent condition: 4.5×10^4 cell cm^{-2}) and 6-well plates (sparse condition: 3.3×10^3 cell cm^{-2}). After 20 hr of incubation, the media were replaced with

Medium 199 with 100 units mL^{-1} penicillin, 100 μg mL^{-1} streptomycin, and 1% BSA with 1 μM PD153035 (EGFR inhibitor) without removing the culture insert. The cells were imaged every 5 min and treated with 2.5 ng mL^{-1} HGF 2.5 hr after the start of imaging. For the analysis of ERK activity in each cell, cells were tracked by TrackMate (Tinevez et al., 2017) by using time-lapse image of CFP (EKARrEV-NLS) as an input of the program.

Lamellipodia induction by SLIPT

Self-localizing ligand-induced protein translocation (SLIPT) approach was reported previously (Suzuki et al., 2022). m^{D}cTMP was synthesized as described previously (Nakamura et al., 2020). MDCK cells expressing EKARrEV-NLS, mCherry-HRasCT, and miRFP703-^{iK6}DHFR-Tiam1(DH-PH) (9.8×10^2 cells) and MDCK cells expressing only EKARrEV-NLS (9.8×10^3 cells) were mixed and seeded into the 2-well culture insert placed on a glass-bottom dish coated with 0.3 mg mL^{-1} type I collagen. After 20 hr of incubation, the cells were released for migration by removing the culture insert and changing the medium to Medium 199 supplemented with 100 units mL^{-1} penicillin and 100 μg mL^{-1} streptomycin with or without 2.5 ng mL^{-1} HGF. The cells were treated with 0.1% DMSO or 10 μM m^{D}cTMP to induce the translocation of miRFP703-^{iK6}DHFR-Tiam1(DH-PH) to the plasma membrane. For the single cell analysis of ERK activity, cells were tracked with TrackMate by using time-lapse image of CFP (EKARrEV-NLS) as an input of the program. Then, the ERK activity change upon the drug treatment was evaluated by the time-lapse data obtained from mCherry-positive cells.

Immunofluorescence and confocal microscopy

MDCK cells were subjected to immunofluorescence analysis as described previously (Hino et al., 2020). Briefly, cells were fixed with 4% paraformaldehyde in PBS for 15 min at room temperature, followed by permeabilization with 0.2% Triton X-100 in PBS for 5 min. The samples were treated with 1% BSA in PBS for 1 hr at room temperature for blocking, followed by sequential incubation with primary and secondary antibodies diluted with 1% BSA in PBS overnight at 4°C (primary antibodies) and for 1-2 hr at room temperature (secondary antibodies). Images were collected using an SP8 confocal microscope (Leica, Wetzlar, Germany).

For the detection of cell surface Met, cells were fixed with 4% paraformaldehyde in PBS for 15 min at room temperature, followed by blocking with 1% BSA in PBS for 1 hr without permeabilization. The samples were sequentially incubated with primary (anti-canine Met goat antibody) and secondary antibodies (alexa 568-conjugated donky anti-goat IgG (H+L) antibody) diluted with 1% BSA in PBS overnight at 4°C (primary antibodies) and for 1 hr at room temperature (secondary antibodies).

Image processing for the FRET/CFP ratio

Image processing for FRET/CFP ratio images was performed with Fiji. The background intensity was subtracted by using the subtract-background function and subsequently processed with a median filter to reduce noise. The processed images were subjected to image calculation and the ratio values were binned into 8 steps to obtain 8-color FRET/CFP ratio

images. To convey the brightness of the original images to the FRET/CFP ratio images, the 8-color FRET/CFP ratio images were multiplied by the corresponding intensity-normalized grayscale image. For the 8 bit pseudocolor FRET/CFP ratio images, CFP images were subjected to thresholding with the Huang method by Fiji to obtain binary images of the nucleus. Then, ratio images without binning of the ratio values were multiplied by the binary images of the nucleus to remove signals in the cell-free regions.

HGF incorporation assay

Recombinant human HGF was prepared from a conditioned medium of CHO cells stably expressing human HGF as described previously (Sakai et al., 2019). Secreted HGF was purified by a HiTrap Heparin HP column (Cytiva), a Superdex 200 Increase 10/300 GL column (Cytiva, Marlborough, MA), and a Sephadex G-25 column (Cytiva) equilibrated with PBS. HGF was labeled with 5-(and-6)-Carboxytetramethylrhodamine, Succinimidyl Ester (Thermo Fisher Scientific) and purified by a Sephadex G-25 column (Cytiva) equilibrated with PBS.

Cells expressing EKARrEV-NLS and miRFP670-HRasCT were prepared for the confinement release assay as described above. After removing the culture insert, cells were subjected to confocal microscopy over a 1-hr time interval and Rhodamine-HGF (final 2.5 ng mL^{-1}) was added 1.5 hr after the start of imaging. Obtained z-stack Rhodamine-HGF images were processed by background subtraction and z-projection by summation of slices. Cell segmentation was performed by Cellpose, a generalist algorithm for cellular segmentation (Stringer et al., 2021), by using the images of nuclei (EKARrEV-NLS) and the plasma membrane (miRFP670-HRasCT) as inputs after maximum projection of the z-stack images. The HGF intensity in each cell was collected and analyzed by using MATLAB.

HGF binding to cell surface

Parent MDCK cells without exogenous gene expression were prepared for the confinement release assay. Three hours after removing the culture insert, the cells were treated with 2 μM PD153035 and incubated further for 3 hr. Then, the medium was exchanged with ice-cold Medium 199 containing 100 units mL^{-1} penicillin, 100 μg mL^{-1} streptomycin, 1% BSA, 2 μM PD153035, and 20 ng mL^{-1} Rhodamine-HGF, and the cells were kept on ice for 10 min to inhibit endocytosis. The cells were fixed with ice-cold 4% paraformaldehyde in PBS for 30 min on ice, followed by permeabilization with 0.2% Triton X-100 in PBS for 5 min at room temperature. The samples were treated with 1% BSA in PBS for 1 hr at room temperature for blocking, followed by sequential incubation with primary (anti-EGF Receptor rabbit antibody) and secondary antibodies (alexa 647-conjugated goat anti-rabbit IgG (H+L) antibody) diluted with 1% BSA in PBS overnight at 4°C (primary antibodies) and for 1 hr at room temperature (secondary antibodies). Images were collected using the SP8 confocal microscope.

Light-induced ERK activation

MDCK cells expressing both EKAREV-NLS and 2paRAF were seeded in a culture insert as described in the confinement release assay section. After 20 hr of incubation, the culture insert

was removed, and the culture media were changed to Medium 199 supplemented with 100 unit mL^{-1} penicillin, 100 μg mL^{-1} streptomycin, 1% BSA, and 1 μM PD153035 with other chemicals as indicated in the figure legends. During the observation, CRY2 was activated with excitation light for CFP imaging at an interval of 5 min to trigger Raf1 activation.

Traction force microscopy

Polyacrylamide gel substrates with 3 kPa stiffness were prepared as previously described, with slight modifications (Rodrı´guez-Franco et al., 2017). Briefly, glass-bottom dishes (IWAKI, Shizuoka, Japan) were treated with 2% acetic acid (WAKO) and 0.2% 3-(trimethoxysilyl)propyl methacrylate (SIGMA) in 80% ethanol for 2 min. After removing the solution, the dishes were dried for 15 min. Acrylamide solution containing 5.5% acrylamide, 0.09% bisacrylamide, 0.05% ammonium persulfate, 0.05% N,N,N',N'-tetramethyl ethylenediamine, and 0.01% red fluorescent carboxylate-modified beads (0.2 mm diameter, F8810; Thermo Fisher Scientific) in PBS were prepared. 18 μL of the solution was placed on the glass-bottom dishes and 18 mm coverslips (Matsunami, Osaka, Japan) were placed on top of the dishes. The methodology of collagen-coating of the gels was described in detail previously (Hino et al., 2020). Images of the beads were collected with the IX81 microscope equipped with a 560DF15 excitation filter (Omega Optical, Brattleboro, VT), a U-MWIGA3 dichromatic mirror, and an FF01-624/40-25 (Semrock) emission filter. Traction forces were computed by Fourier-transform traction microscopy as described previously (Trepat et al., 2009). Traction forces under leader cells were collected from the circular regions with 50 μm radii located at the center of mass of leader cell nuclei.

QUANTIFICATION AND STATISTICAL ANALYSIS

Quantification of ERK activation

To obtain heatmaps of ERK activity in leader and follower cells, the FRET/CFP ratio images were cropped to obtain regions with a length of 140 μm along the y-axis. Values of the FRET/CFP ratio were averaged along the y-axis in each region, providing intensity lines along the x-axis. The operation was repeated for the respective time points, and the intensity lines were stacked along the y-axis for all time points to obtain the kymographs of the FRET/CFP ratio images for each region. For the quantification of ERK activity by the region-based method, the values of the FRET/CFP ratio at the leading edge of the migrating cell group in the kymographs were defined as ERK activity in leader cells. Also, the values of the FRET/CFP ratio at the region 200 μm distant from the leading edge were defined as ERK activity in follower cells.

For the quantification of ERK activity by a single cell-based method, segmentation of the nucleus was performed by the Huang thresholding method, and the mean values of the FRET/CFP ratio in each cell were collected from the segmented nuclei. The FRET/CFP ratio images were cropped to obtain regions with a length of 45 μm along the y-axis, and the values of the FRET/CFP ratio in the cells at the head of the migration cell group in each region were defined as ERK activity in leader cells. Then, the values of the FRET/CFP ratio in the cells

200–230 μm distant from the leader cells in each region were defined as ERK activity in follower cells.

Quantification of Ras activation

For the live-cell imaging of Ras activity in each cell, cells with and without the expression of Raichu-Ras-HRasCT were seeded into a 2-well culture insert at a ratio of 1:10 (in total 9.8×10^3 cells) to prepare mosaic monolayers. The cells were imaged as described above in the confinement release assay section. For the quantification of Ras activity, the images of Raichu-Ras-HRasCT were used for cell segmentation by Cellpose. The segmented cells were divided into two parts at the center of mass of the segmented cell to define the cell front and rear. Ras activity in each region was collected and analyzed by MATLAB.

Quantification of cell area and FAs

For the quantification of cell area, z-stack images of nuclei (EKARrEV-NLS) and miRFP670-HRasCT fluorescence or paxillin immunostaining were subjected to maximum projection. The processed images were used for the cell segmentation by Cellpose. Analysis of the cell area was performed by MATLAB.

For the analysis of FA intensity, planes of focal adhesions were manually selected from the z-stack images of paxillin immunostaining after background subtraction. The images of focal adhesion planes were subjected to maximum projection and then Moments thresholding to segment regions of FAs. The total intensity (integrated density) of the paxillin signals within the segmented FAs was collected and analyzed by MATLAB. The images of segmented cells created by Cellpose were used to obtain the paxillin intensity at FAs in each cell.

Statistical analysis

Statistical analyses were performed with GraphPad Prism 7 or 9 software (GraphPad Software, San Diego, CA). No statistical analysis was used to predetermine the sample size. The sample sizes, statistical tests, and p-values are indicated in the figures and the figure legends. p-values were classified as follows: *p<0.05, **p<0.01, ***p<0.001, ****p<0.0001, and n.s. (not significant, i.e., p>0.05).

Supplemental video titles and legends

Video S1. ERK activity dynamics during collective cell migration, Related to Figure 1.

Time-lapse video of collectively migrating MDCK cells expressing EKAREV-NLS. The color represents the FRET/CFP ratio, which indicates ERK activity (top). DIC images are shown at the bottom. The color-code corresponds to that in Figure 1B.

Video S2. ERK activation in leader cells is independent of EGFR activity, Related to Figure 1.

Time-lapse video of collectively migrating MDCK cells. The color represents the FRET/CFP ratio, which indicates ERK activity. The cells were treated with DMSO (upper) or 2 μM PD153035 (EGFR inhibitor; lower) at 3.5 hr. The ratio range is 1.10 to 1.55.

Video S3. ERK activation in leader cells requires FBS, Related to Figure 2.

Time-lapse video of collectively migrating MDCK cells in the media with (left) or without (right) FBS. The cells were treated with 2 μM PD153035 (EGFR inhibitor; lower) at 3.5 hr. The color represents the FRET/CFP ratio, which indicates ERK activity. The color-code corresponds to that in Figure 2A.

Video S4. Met expression is required for the sustained ERK activation in leader cells, Related to Figure 2.

Time-lapse videos of collectively migrating WT (upper), Met KO clone #1 (middle), and Met KO clone #2 (lower) MDCK cells in the FBS-containing media. The cells were treated with 2 μM PD153035 (EGFR inhibitor) at 3.5 hr. The color-code corresponds to that in Figure 2H.

Video S5. HGF causes Ras activation exclusively at the lamellipodia of leader cells, Related to Figure 4.

Time-lapse video of migrating follower (left) and leader (right) cells expressing Raichu-Ras-HRasCT in 2 μM PD153035 (EGFR inhibitor)-containing media supplemented with (lower) or without (upper) 2.5 ng mL^{-1} HGF. The color represents the FRET/CFP ratio, which indicates Ras activity. The color-code corresponds to that in Figure 4A.

Video S6. The sustained ERK activation in leader cells is not affected by disruption of the adherens junction, Related to Figure 5.

Time-lapse videos of collectively migrating WT (upper), α-1-catenin KO clone #1 (middle), and α-1-catenin KO clone #2 (lower) MDCK cells in the FBS-containing media. The cells were treated with 2 μM PD153035 (EGFR inhibitor) at 3.5 hr. The color-code corresponds to that in Figure 5A.

Video S7. The release from confinement is prerequisite for the sustained ERK activation in leader cells, Related to Figure 5.

Time-lapse video of migrating (left) or confined (right) MDCK cells. The cells were treated with 2 μM PD153035 (EGFR inhibitor) at 3.5 hr. The color-code corresponds to that in Figure 5E.

Video S8. Talin1 expression is required for the sustained ERK activation in the leader cells, Related to Figure 6.

Time-lapse videos of collectively migrating WT (upper), talin1 KO clone #1 (middle), and talin1 KO clone #2 (lower) MDCK cells in the FBS-containing media. The cells were treated with 2 μM PD153035 (EGFR inhibitor) at 3.5 hr. The color-code corresponds to that in Figure 6F.

Video S9. Optogenetic ERK activation promotes lamellipodial extension in an Arp2/3-dependent manner, Related to Figure 7.

Time-lapse videos of MDCK cells expressing 2paRAF in serum-free media with 2 μM PD153035 (EGFR inhibitor) as well as 0.1% DMSO (left), 200 nM trametinib (MEK inhibitor, center), or 100 μM CK666 (Arp2/3 inhibitor, right). The images represent the fluorescence of CIBN-mScarlet-I-CAAX, a component of 2paRAF. The blue light illumination for the photoactivation of Raf1 is started at 4 hr.

References

Amano, M., Ito, M., Kimura, K., Fukata, Y., Chihara, K., Nakano, T., Matsuura, Y., and Kaibuchi, K. (1996). Phosphorylation and activation of myosin by Rho-associated kinase (Rho-kinase). Journal of Biological Chemistry *271*, 20246-20249.

Aoki, K., Kondo, Y., Naoki, H., Hiratsuka, T., Itoh, R.E., and Matsuda, M. (2017). Propagating wave of ERK activation orients collective cell migration. Dev Cell *43*, 305-317 e305.

Aoki, K., Kumagai, Y., Sakurai, A., Komatsu, N., Fujita, Y., Shionyu, C., and Matsuda, M. (2013). Stochastic ERK activation induced by noise and cell-to-cell propagation regulates cell density-dependent proliferation. Mol Cell *52*, 529-540.

Aoki, K. and Matsuda, M. (2009). Visualization of small GTPase activity with fluorescence resonance energy transfer-based biosensors. Nature Protocols *4*, 1623-1631.

Barriga, E.H., Franze, K., Charras, G., and Mayor, R. (2018). Tissue stiffening coordinates morphogenesis by triggering collective cell migration in vivo. Nature *554*, 523-527.

Boocock, D., Hino, N., Ruzickova, N., Hirashima, T., and Hannezo, E. (2020). Theory of mechanochemical patterning and optimal migration in cell monolayers. Nature Physics *17*, 267-274.

Burridge, K., and Guilluy, C. (2016). Focal adhesions, stress fibers and mechanical tension. Experimental cell research *343*, 14-20.

Cai, D., Chen, S.C., Prasad, M., He, L., Wang, X., Choesmel-Cadamuro, V., Sawyer, J.K., Danuser, G., and Montell, D.J. (2014). Mechanical feedback through E-cadherin promotes direction sensing during collective cell migration. Cell *157*, 1146-1159.

Chan, C.J., Heisenberg, C.P., and Hiiragi, T. (2017). Coordination of Morphogenesis and Cell-Fate Specification in Development. Curr Biol *27*, R1024-R1035.

Chmielowiec, J., Borowiak, M., Morkel, M., Stradal, T., Munz, B., Werner, S., Wehland, J., Birchmeier, C., and Birchmeier, W. (2007). c-Met is essential for wound healing in the skin. J Cell Biol *177*, 151-162.

Chu, C.L., Buczek-Thomas, J.A., and Nugent, M.A. (2004). Heparan sulphate proteoglycans modulate fibroblast growth factor-2 binding through a lipid raft-mediated mechanism. The Biochemical journal *379*, 331-341.

Chung, I., Akita, R., Vandlen, R., Toomre, D., Schlessinger, J., and Mellman, I. (2010). Spatial control of EGF receptor activation by reversible dimerization on living cells. Nature *464*, 783-787.

Das, T., Safferling, K., Rausch, S., Grabe, N., Boehm, H., and Spatz, J.P. (2015). A molecular mechanotransduction pathway regulates collective migration of epithelial cells. Nat Cell Biol *17*, 276-287.

Derksen, P.W., Keehnen, R.M., Evers, L.M., van Oers, M.H., Spaargaren, M., and Pals, S.T. (2002). Cell surface proteoglycan syndecan-1 mediates hepatocyte growth factor binding and promotes Met signaling in multiple myeloma. Blood *99*, 1405-1410.

Duchek, P., and Rorth, P. (2001). Guidance of cell migration by EGF receptor signaling during Drosophila oogenesis. Science *291*, 131-133.

Durdu, S., Iskar, M., Revenu, C., Schieber, N., Kunze, A., Bork, P., Schwab, Y., and Gilmour, D. (2014). Luminal signalling links cell communication to tissue architecture during organogenesis. Nature *515*, 120-124.

Elfenbein, A., Lanahan, A., Zhou, T.X., Yamasaki, A., Tkachenko, E., Matsuda, M., and Simons, M. (2012). Syndecan 4 regulates FGFR1 signaling in endothelial cells by directing macropinocytosis. Sci Signal *5*, ra36.

Ephstein, Y., Singleton, P.A., Chen, W., Wang, L., Salgia, R., Kanteti, P., Dudek, S.M., Garcia, J.G., and Jacobson, J.R. (2013). Critical role of S1PR1 and integrin beta4 in HGF/c-Met-mediated increases in vascular integrity. J Biol Chem *288*, 2191-2200.

Farooqui, R., and Fenteany, G. (2005). Multiple rows of cells behind an epithelial wound edge extend cryptic lamellipodia to collectively drive cell-sheet movement. J Cell Sci *118*, 51-63.

Friedl, P., and Gilmour, D. (2009). Collective cell migration in morphogenesis, regeneration and cancer. Nat Rev Mol Cell Biol *10*, 445-457.

Gerhardt, H., Golding, M., Fruttiger, M., Ruhrberg, C., Lundkvist, A., Abramsson, A., Jeltsch, M., Mitchell, C., Alitalo, K., Shima, D.*, et al.* (2003). VEGF guides angiogenic sprouting utilizing endothelial tip cell filopodia. J Cell Biol *161*, 1163-1177.

Guillemot, L., Guerrera, D., Spadaro, D., Tapia, R., Jond, L., and Citi, S. (2014). MgcRacGAP interacts with cingulin and paracingulin to regulate Rac1 activation and development of the tight junction barrier during epithelial junction assembly. Mol Biol Cell *25*, 1995-2005.

Gutierrez, J., Cabrera, D., and Brandan, E. (2014). Glypican-1 regulates myoblast response to HGF via Met in a lipid raft-dependent mechanism: effect on migration of skeletal muscle precursor cells. Skelet Muscle *4*, 5.

Hammond, D.E., Carter, S., McCullough, J., Urbe, S., Vande Woude, G., and Clague, M.J. (2003). Endosomal dynamics of Met determine signaling output. Mol Biol Cell *14*, 1346-1354.

Hannezo, E., and Heisenberg, C.-P. (2019). Mechanochemical feedback loops in development and disease. Cell *178*, 12-25.

Harvey, C.D., Ehrhardt, A.G., Cellurale, C., Zhong, H., Yasuda, R., Davis, R.J., and Svoboda, K. (2008). A genetically encoded fluorescent sensor of ERK activity. Proc Natl Acad Sci U S A *105*, 19264-19269.

Hino, N., Rossetti, L., Marin-Llaurado, A., Aoki, K., Trepat, X., Matsuda, M., and Hirashima, T. (2020). ERK-mediated mechanochemical waves direct collective cell polarization. Dev Cell *53*, 646-660 e648.

Hiratsuka, T., Fujita, Y., Naoki, H., Aoki, K., Kamioka, Y., and Matsuda, M. (2015). Intercellular propagation of extracellular signal-regulated kinase activation revealed by in vivo imaging of mouse skin. eLife *4*, e05178.

Jakobsson, L., Kreuger, J., Holmborn, K., Lundin, L., Eriksson, I., Kjellen, L., and Claesson-Welsh, L. (2006). Heparan sulfate in trans potentiates VEGFR-mediated angiogenesis. Dev Cell *10*, 625-634.

Jansen, K.A., Donato, D.M., Balcioglu, H.E., Schmidt, T., Danen, E.H., and Koenderink, G.H. (2015). A guide to mechanobiology: Where biology and physics meet. Biochim Biophys Acta *1853*, 3043-3052.

Kalappurakkal, J.M., Anilkumar, A.A., Patra, C., van Zanten, T.S., Sheetz, M.P., and Mayor, S. (2019). Integrin Mechano-chemical Signaling Generates Plasma Membrane Nanodomains that Promote Cell Spreading. Cell.

Khalil, A.A., and Friedl, P. (2010). Determinants of leader cells in collective cell migration. Integr Biol (Camb) *2*, 568-574.

Kim, K.B., Yi, J.S., Nguyen, N., Lee, J.H., Kwon, Y.C., Ahn, B.Y., Cho, H., Kim, Y.K., Yoo, H.J., Lee, J.S.*, et al.* (2011). Cell-surface receptor for complement component C1q (gC1qR) is

a key regulator for lamellipodia formation and cancer metastasis. J Biol Chem *286*, 23093-23101.

Kimura, K., Ito, M., Amano, M., Chihara, K., Fukata, Y., Nakafuku, M., Yamamori, B., Feng, J., Nakano, T., Okawa, K.*, et al.* (1996). Regulation of myosin phosphatase by Rho and Rho-associated kinase (Rho-kinase). Science *273*, 245-248.

Kinjo, T., Terai, K., Horita, S., Nomura, N., Sumiyama, K., Togashi, K., Iwata, S., and Matsuda, M. (2019). FRET-assisted photoactivation of flavoproteins for in vivo two-photon optogenetics. Nat Methods *16*, 1029-1036.

Komatsu, N., Aoki, K., Yamada, M., Yukinaga, H., Fujita, Y., Kamioka, Y., and Matsuda, M. (2011). Development of an optimized backbone of FRET biosensors for kinases and GTPases. Mol Biol Cell *22*, 4647-4656.

Komatsu, N., Terai, K., Imanishi, A., Kamioka, Y., Sumiyama, K., Jin, T., Okada, Y., Nagai, T., and Matsuda, M. (2018). A platform of BRET-FRET hybrid biosensors for optogenetics, chemical screening, and in vivo imaging. Sci Rep *8*, 8984.

Li, J.F., Duan, H.F., Wu, C.T., Zhang, D.J., Deng, Y., Yin, H.L., Han, B., Gong, H.C., Wang, H.W., and Wang, Y.L. (2013). HGF accelerates wound healing by promoting the dedifferentiation of epidermal cells through beta1-integrin/ILK pathway. Biomed Res Int *2013*, 470418.

Li, N., Gao, W., Zhang, Y.F., and Ho, M. (2018). Glypicans as Cancer Therapeutic Targets. Trends Cancer *4*, 741-754.

Li, S., Gerrard, E.R., Jr., and Balkovetz, D.F. (2004). Evidence for ERK1/2 phosphorylation controlling contact inhibition of proliferation in Madin-Darby canine kidney epithelial cells. American journal of physiology Cell physiology *287*, C432-439.

Lin, S., Hirayama, D., Maryu, G., Matsuda, K., Hino, N., Deguchi, E., Aoki, K., Iwamoto, R., Terai, K., and Matsuda, M. (2022). Redundant roles of EGFR ligands in the ERK activation waves during collective cell migration. Life Sci Alliance *5*.

Liu, Y., Chattopadhyay, N., Qin, S., Szekeres, C., Vasylyeva, T., Mahoney, Z.X., Taglienti, M., Bates, C.M., Chapman, H.A., Miner, J.H.*, et al.* (2009). Coordinate integrin and c-Met signaling regulate Wnt gene expression during epithelial morphogenesis. Development (Cambridge, England) *136*, 843-853.

Machide, M., Hashigasako, A., Matsumoto, K., and Nakamura, T. (2006). Contact inhibition of hepatocyte growth regulated by functional association of the c-Met/hepatocyte growth factor receptor and LAR protein-tyrosine phosphatase. J Biol Chem *281*, 8765-8772.

Manes, S., Mira, E., Gomez-Mouton, C., Lacalle, R.A., Keller, P., Labrador, J.P., and Martinez, A.C. (1999). Membrane raft microdomains mediate front-rear polarity in migrating cells. EMBO J *18*, 6211-6220.

Matsubayashi, Y., Ebisuya, M., Honjoh, S., and Nishida, E. (2004). ERK activation propagates in epithelial cell sheets and regulates their migration during wound healing. Curr Biol *14*, 731-735.

Mayor, R., and Etienne-Manneville, S. (2016). The front and rear of collective cell migration. Nat Rev Mol Cell Biol *17*, 97-109.

McDonald, J.A., Pinheiro, E.M., and Montell, D.J. (2003). PVF1, a PDGF/VEGF homolog, is sufficient to guide border cells and interacts genetically with Taiman. Development (Cambridge, England) *130*, 3469-3478.

Mendonsa, A.M., Na, T.Y., and Gumbiner, B.M. (2018). E-cadherin in contact inhibition and cancer. Oncogene *37*, 4769-4780.

Miura, Y., Ngo Thai Bich, V., Furuya, M., Hasegawa, H., Takahashi, S., Katagiri, N., Hongu, T., Funakoshi, Y., Ohbayashi, N., and Kanaho, Y. (2017). The small G protein Arf6 expressed in keratinocytes by HGF stimulation is a regulator for skin wound healing. Sci Rep *7*, 46649.

Mizuno, K., Higuchi, O., Tajima, H., Yonemasu, T., and Nakamura, T. (1993). Cell density-dependent regulation of hepatocyte growth factor receptor on adult rat hepatocytes in primary culture. J Biochem *114*, 96-102.

Mochizuki, N., Yamashita, S., Kurokawa, K., Ohba, Y., Nagai, T., Miyawaki, A., and Matsuda, M. (2001). Spatio-temporal images of growth-factor-induced activation of Ras and Rap1. Nature *411*, 1065-1068.

Montesano, R., Matsumoto, K., Nakamura, T., and Orci, L. (1991a). Identification of a fibroblast-derived epithelial morphogen as hepatocyte growth factor. Cell *67*, 901-908.

Montesano, R., Schaller, G., and Orci, L. (1991b). Induction of epithelial tubular morphogenesis in vitro by fibroblast-derived soluble factors. Cell *66*, 697-711.

Morgan, M.R., Humphries, M.J., and Bass, M.D. (2007). Synergistic control of cell adhesion by integrins and syndecans. Nat Rev Mol Cell Biol *8*, 957-969.

Naito, Y., Hino, K., Bono, H., and Ui-Tei, K. (2015). CRISPRdirect: software for designing CRISPR/Cas guide RNA with reduced off-target sites. Bioinformatics (Oxford, England) *31*, 1120-1123.

Nakahara, S., Tsutsumi, K., Zuinen, T., and Ohta, Y. (2015). FilGAP, a Rho-ROCK-regulated GAP for Rac, controls adherens junctions in MDCK cells. J Cell Sci *128*, 2047-2056.

Nakamura, A., Oki, C., Sawada, S., Yoshii, T., Kuwata, K., Rudd, A.K., Devaraj, N.K., Noma, K., and Tsukiji, S. (2020). Designer Palmitoylation Motif-Based Self-Localizing Ligand for Sustained Control of Protein Localization in Living Cells and Caenorhabditis elegans. ACS Chem Biol *15*, 837-843.

Nakamura, T., and Mizuno, S. (2010). The discovery of hepatocyte growth factor (HGF) and its significance for cell biology, life sciences and clinical medicine. Proc Jpn Acad Ser B Phys Biol Sci *86*, 588-610.

Omelchenko, T., Vasiliev, J.M., Gelfand, I.M., Feder, H.H., and Bonder, E.M. (2003). Rho-dependent formation of epithelial "leader" cells during wound healing. P Natl Acad Sci USA *100*, 10788-10793.

Ornitz, D.M. (2000). FGFs, heparan sulfate and FGFRs: complex interactions essential for development. Bioessays *22*, 108-112.

Ozawa, M., Hiver, S., Yamamoto, T., Shibata, T., Upadhyayula, S., Mimori-Kiyosue, Y., and Takeichi, M. (2020). Adherens junction regulates cryptic lamellipodia formation for epithelial cell migration. J Cell Biol *219*.

Reffay, M., Parrini, M.C., Cochet-Escartin, O., Ladoux, B., Buguin, A., Coscoy, S., Amblard, F., Camonis, J., and Silberzan, P. (2014). Interplay of RhoA and mechanical forces in collective cell migration driven by leader cells. Nat Cell Biol *16*, 217-223.

Riahi, R., Sun, J., Wang, S., Long, M., Zhang, D.D., and Wong, P.K. (2015). Notch1-Dll4 signalling and mechanical force regulate leader cell formation during collective cell migration. Nat Commun *6*, 6556.

Sakai, K., Passioura, T., Sato, H., Ito, K., Furuhashi, H., Umitsu, M., Takagi, J., Kato, Y., Mukai, H., Warashina, S.*, et al.* (2019). Macrocyclic peptide-based inhibition and imaging of hepatocyte growth factor. Nat Chem Biol *15*, 598-606.

Sano, T., Kobayashi, T., Ogawa, O., and Matsuda, M. (2018). Gliding Basal Cell Migration of the Urothelium during Wound Healing. Am J Pathol *188*, 2564-2573.

Sawano, A., Takayama, S., Matsuda, M., and Miyawaki, A. (2002). Lateral propagation of EGF signaling after local stimulation is dependent on receptor density. Developmental Cell *3*, 245-257.

Schindelin, J., Arganda-Carreras, I., Frise, E., Kaynig, V., Longair, M., Pietzsch, T., Preibisch, S., Rueden, C., Saalfeld, S., Schmid, B.*, et al.* (2012). Fiji: an open-source platform for biological-image analysis. Nat Methods *9*, 676-682.

Stoker, M., Gherardi, E., Perryman, M., and Gray, J. (1987). Scatter Factor Is a Fibroblast-Derived Modulator of Epithelial-Cell Mobility. Nature *327*, 239-242.

Stringer, C., Wang, T., Michaelos, M., and Pachitariu, M. (2021). Cellpose: a generalist algorithm for cellular segmentation. Nat Methods *18*, 100-106.

Suzuki, S., Nakamura, A., Hatano, Y., Yoshikawa, M., Yoshii, T., Sawada, S., Atsuta-Tsunoda, K., Aoki, K., and Tsukiji, S. (2022). A chemogenetic platform for controlling plasma membrane signaling and synthetic signal oscillation. Cell Chem. Biol. *29*, 1446-1464.e1410.

Tambe, D.T., Hardin, C.C., Angelini, T.E., Rajendran, K., Park, C.Y., Serra-Picamal, X., Zhou, E.H., Zaman, M.H., Butler, J.P., Weitz, D.A.*, et al.* (2011). Collective cell guidance by cooperative intercellular forces. Nat Mater *10*, 469-475.

Tinevez, J.Y., Perry, N., Schindelin, J., Hoopes, G.M., Reynolds, G.D., Laplantine, E., Bednarek, S.Y., Shorte, S.L., and Eliceiri, K.W. (2017). TrackMate: An open and extensible platform for single-particle tracking. Methods *115*, 80-90.

Tkachenko, E., and Simons, M. (2002). Clustering induces redistribution of syndecan-4 core protein into raft membrane domains. J Biol Chem *277*, 19946-19951.

Totsukawa, G., Yamakita, Y., Yamashiro, S., Hartshorne, D.J., Sasaki, Y., and Matsumura, F. (2000). Distinct roles of ROCK (Rho-kinase) and MLCK in spatial regulation of MLC phosphorylation for assembly of stress fibers and focal adhesions in 3T3 fibroblasts. J Cell Biol *150*, 797-806.

Trepat, X., Wasserman, M.R., Angelini, T.E., Millet, E., Weitz, D.A., Butler, J.P., and Fredberg, J.J. (2009). Physical forces during collective cell migration. Nature Physics *5*, 426-430.

Vining, K.H., and Mooney, D.J. (2017). Mechanical forces direct stem cell behaviour in development and regeneration. Nat Rev Mol Cell Biol *18*, 728-742.

Viticchie, G., and Muller, P.A.J. (2015). c-Met and Other Cell Surface Molecules: Interaction, Activation and Functional Consequences. Biomedicines *3*, 46-70.

Yamaguchi, N., Mizutani, T., Kawabata, K., and Haga, H. (2015). Leader cells regulate collective cell migration via Rac activation in the downstream signaling of integrin beta1 and PI3K. Sci Rep *5*, 7656.

Yang, J.M., Bhattacharya, S., West-Foyle, H., Hung, C.F., Wu, T.C., Iglesias, P.A., and Huang, C.H. (2018). Integrating chemical and mechanical signals through dynamic coupling between cellular protrusions and pulsed ERK activation. Nat Commun *9*, 4673.

Yi, C., Troutman, S., Fera, D., Stemmer-Rachamimov, A., Avila, J.L., Christian, N., Persson, N.L., Shimono, A., Speicher, D.W., Marmorstein, R.*, et al.* (2011). A tight junction-associated Merlin-angiomotin complex mediates Merlin's regulation of mitogenic signaling and tumor suppressive functions. Cancer Cell *19*, 527-540.

Yusa, K., Rad, R., Takeda, J., and Bradley, A. (2009). Generation of transgene-free induced pluripotent mouse stem cells by the piggyBac transposon. Nat Methods *6*, 363-369.

Figure 1

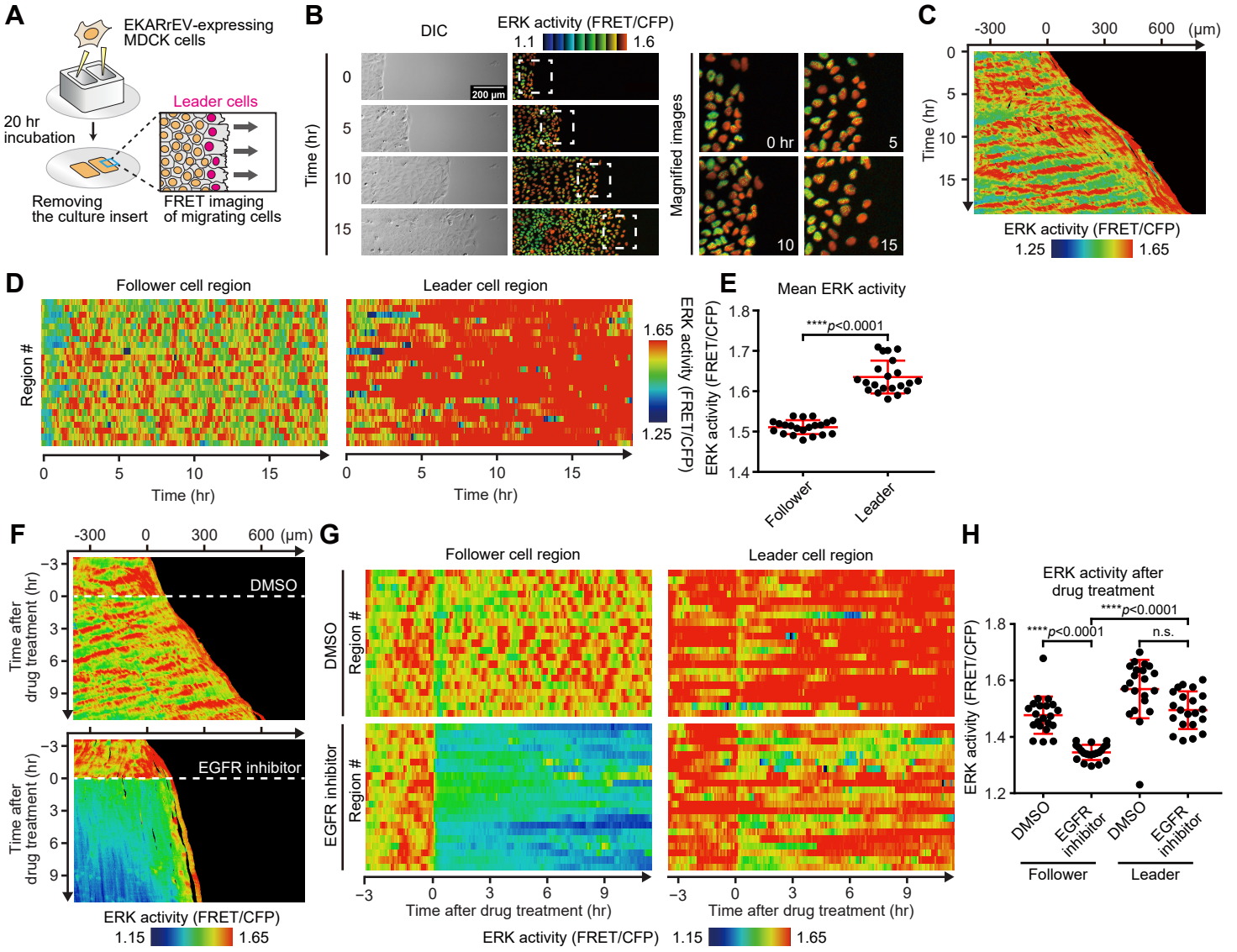

Hino et al.

Figure 2

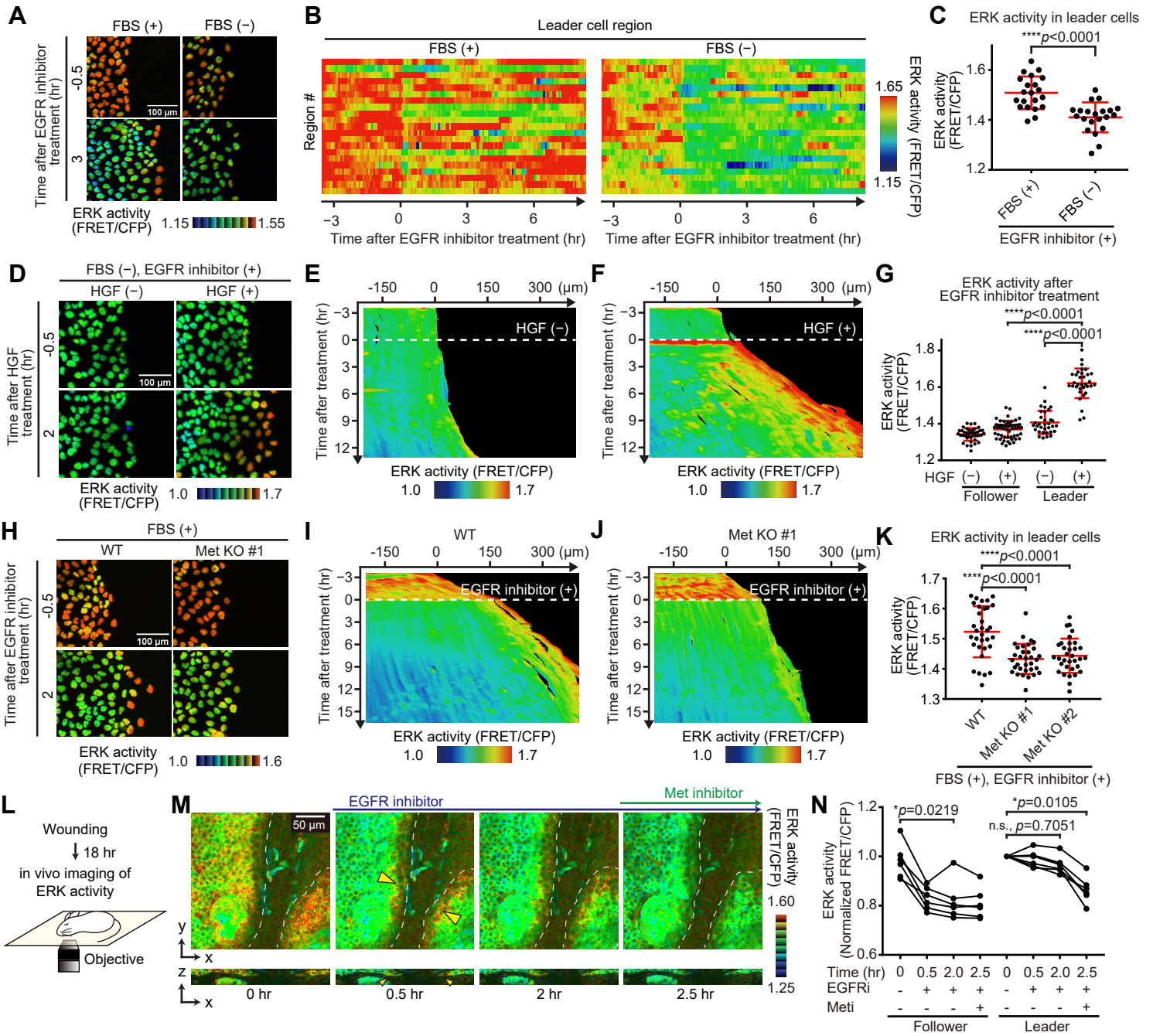

Hino et al.

Figure 3

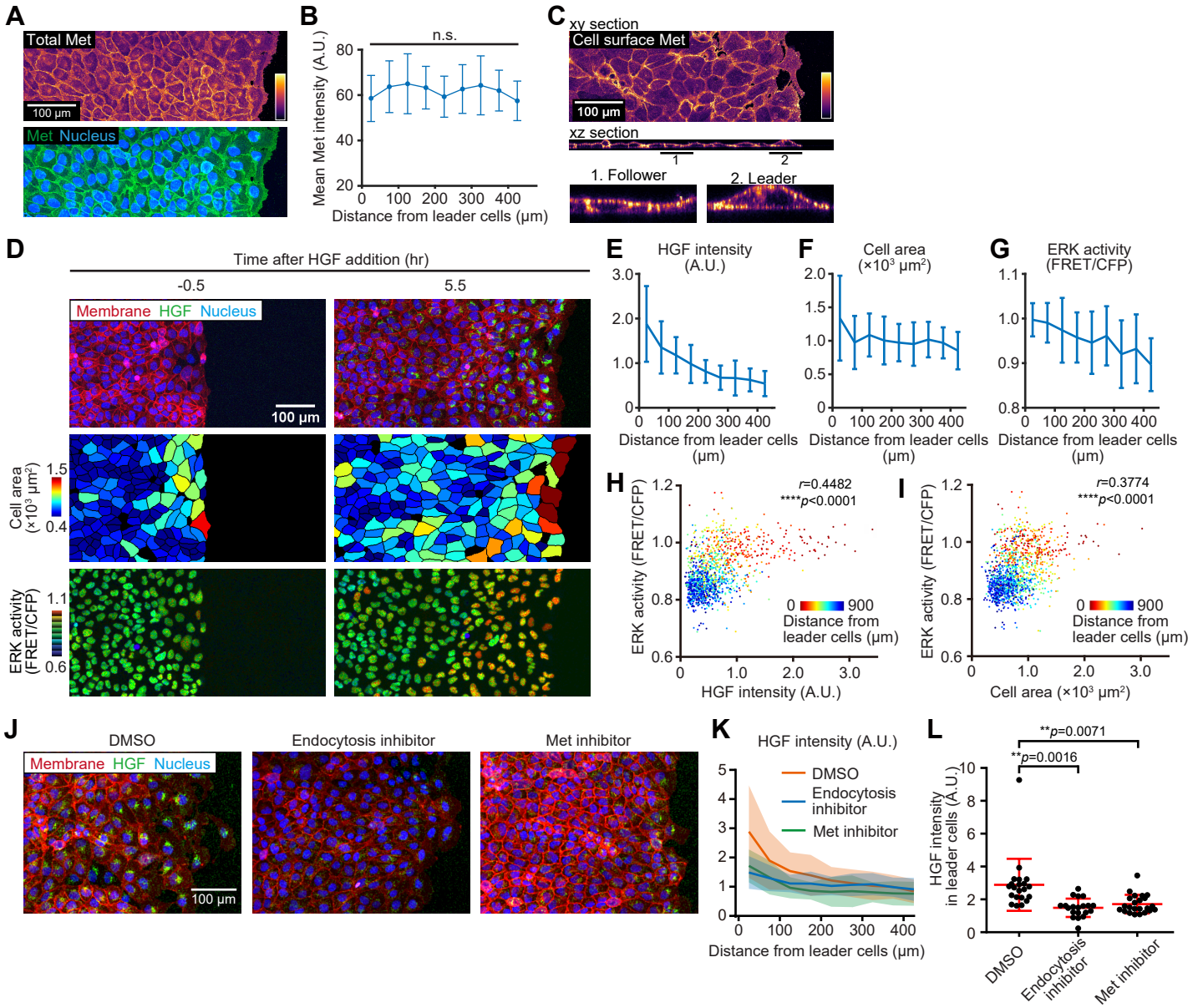

Hino et al.

Figure 4

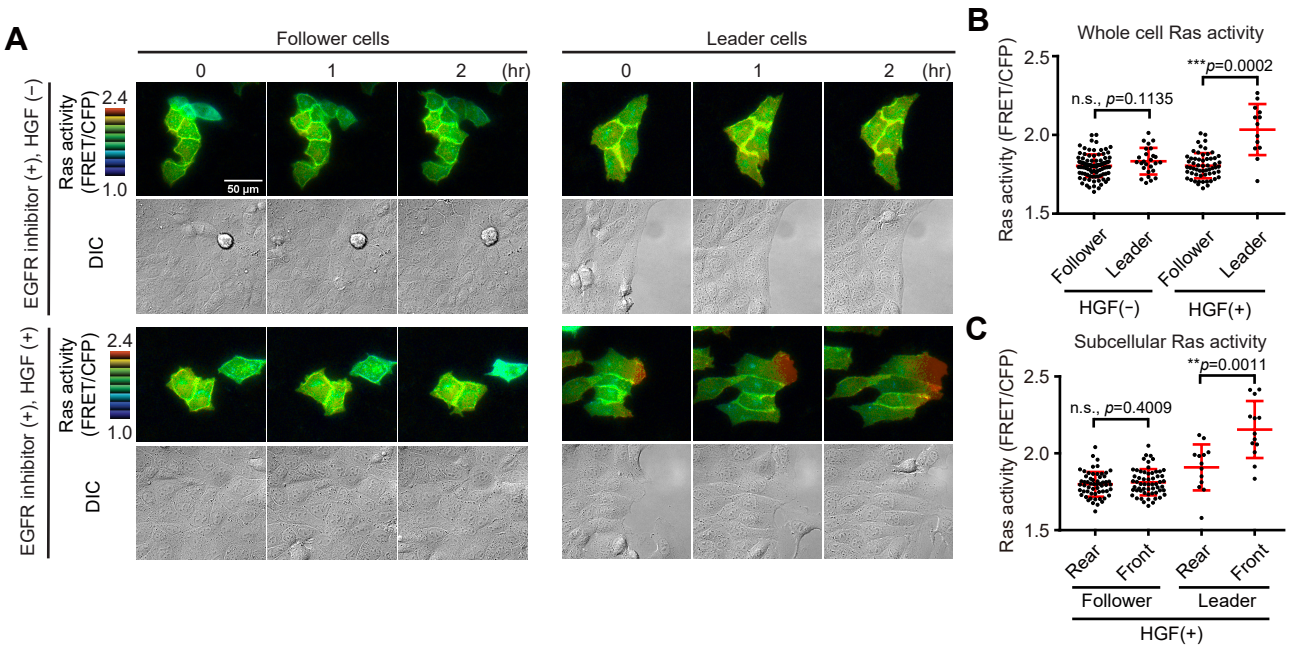

Hino et al.

Figure 5

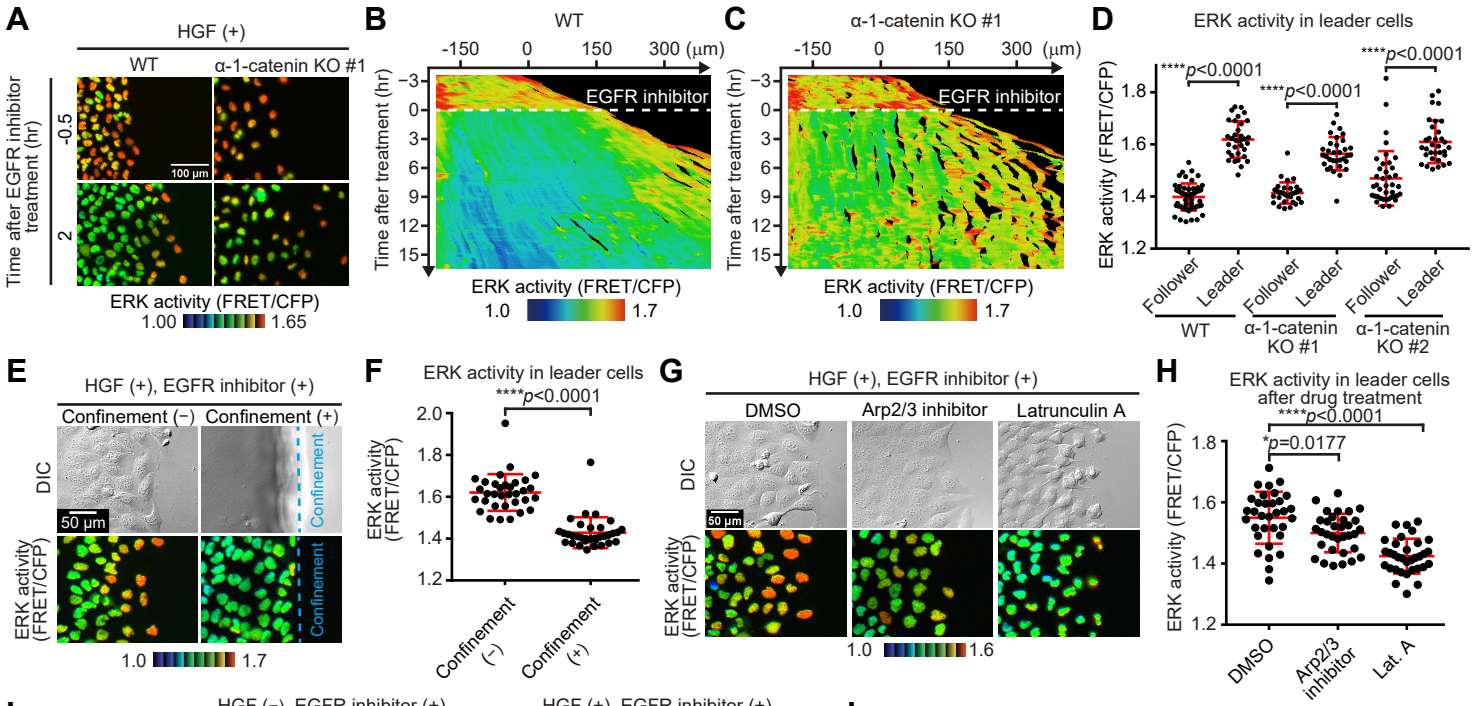

Hino et al.

Figure 6

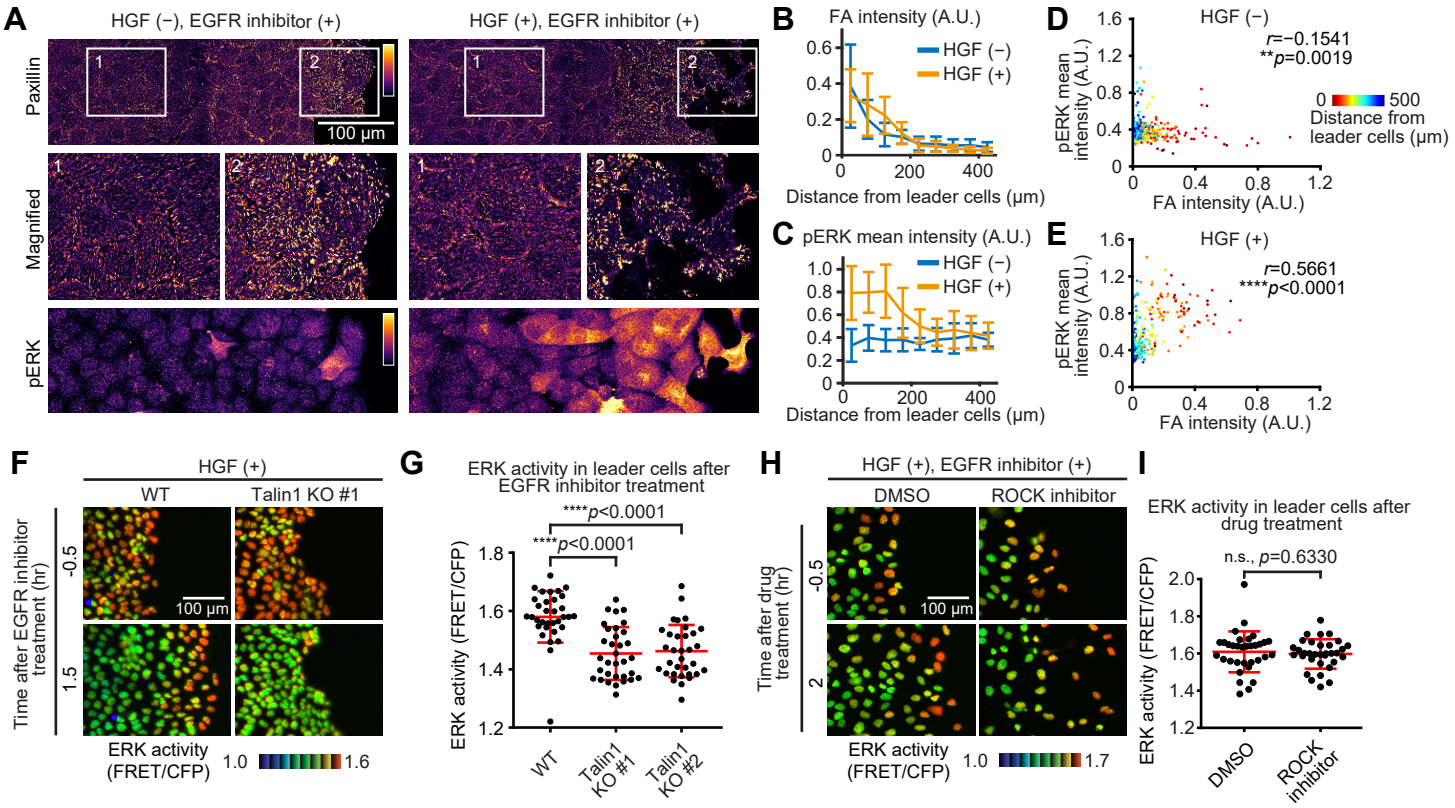

Hino et al.

Figure 7

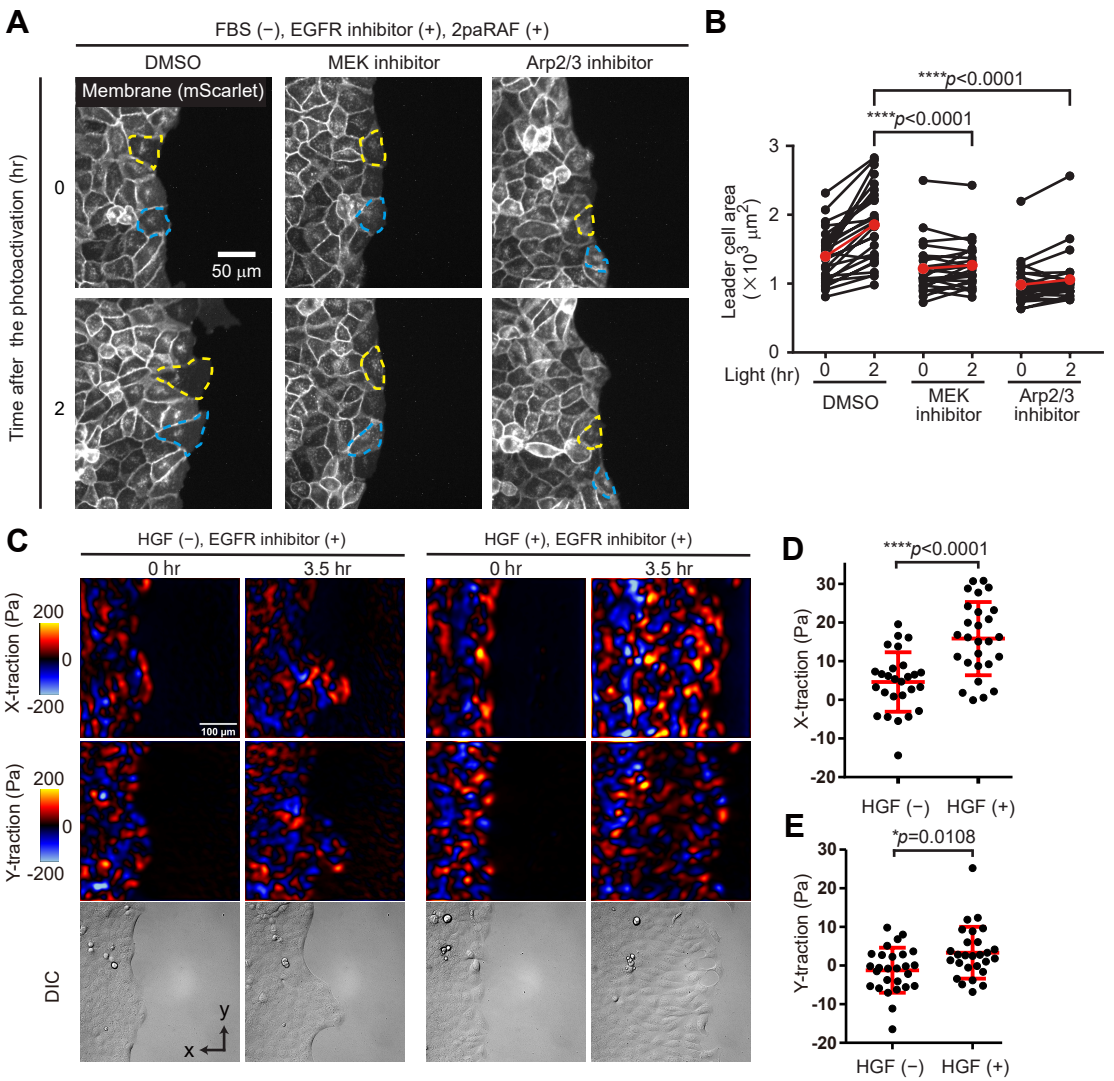

Hino et al.

Figure S1

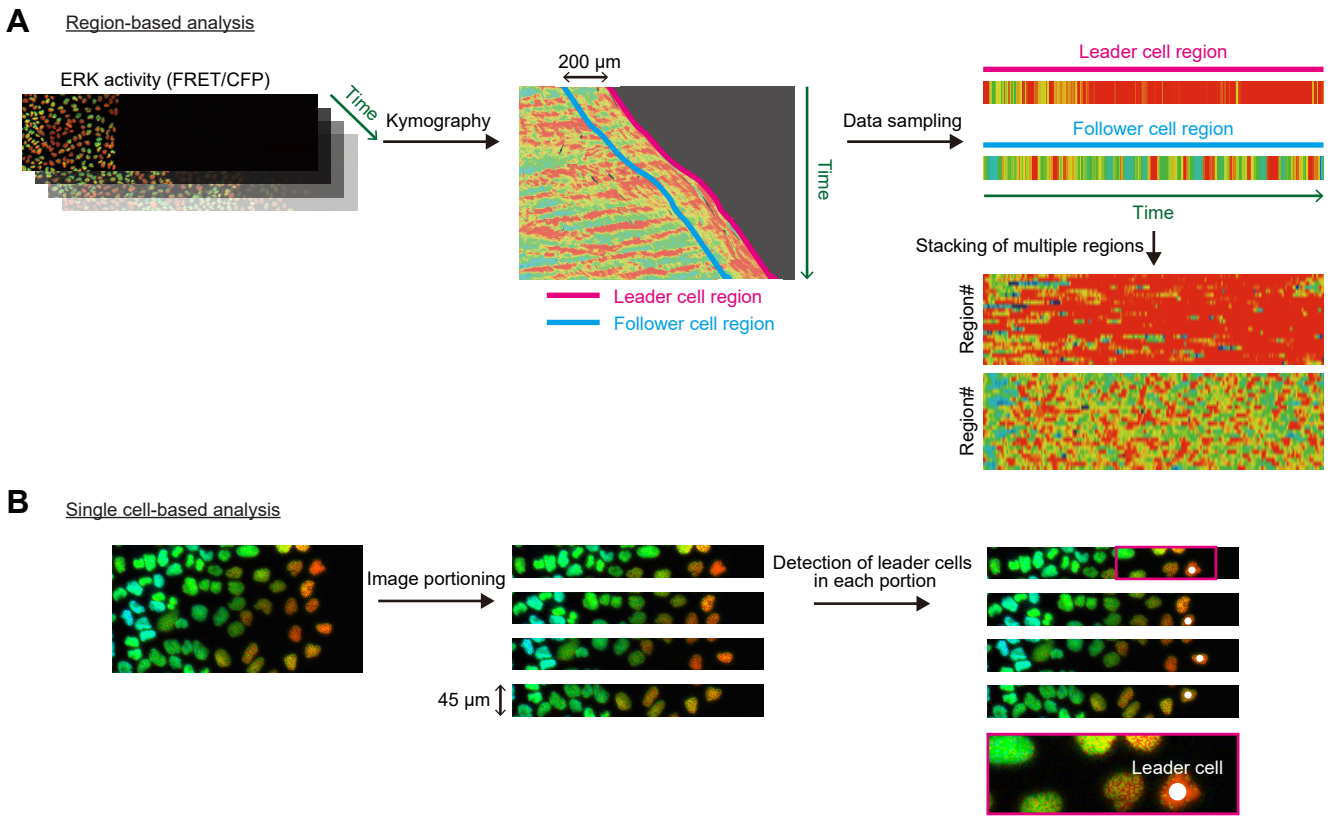

Figure S1. Schematics for the analysis of ERK activity in the leader and follower cells, Related to Figures 1 and 2
(A) Schematics for the region-based analysis of ERK activity. Kymographs are generated from time-lapse FRET/CFP ratio images. The FRET/CFP ratio at the free edge of the migrating cells in the kymographs as indicated by the magenta region was defined as the ERK activity in the leader cells. The FRET/CFP ratio at the region 200 μm distant from the free edge (the cyan region) was defined as the ERK activity in the follower cells.
(B) Schematics for the single cell-based analysis of ERK activity. A snapshot image of FRET/CFP ratio was cropped to obtain regions with a height of 45 μm. The FRET/CFP ratio in the rightmost cell in each region was defined as the ERK activity in the leader cell.

Figure S2

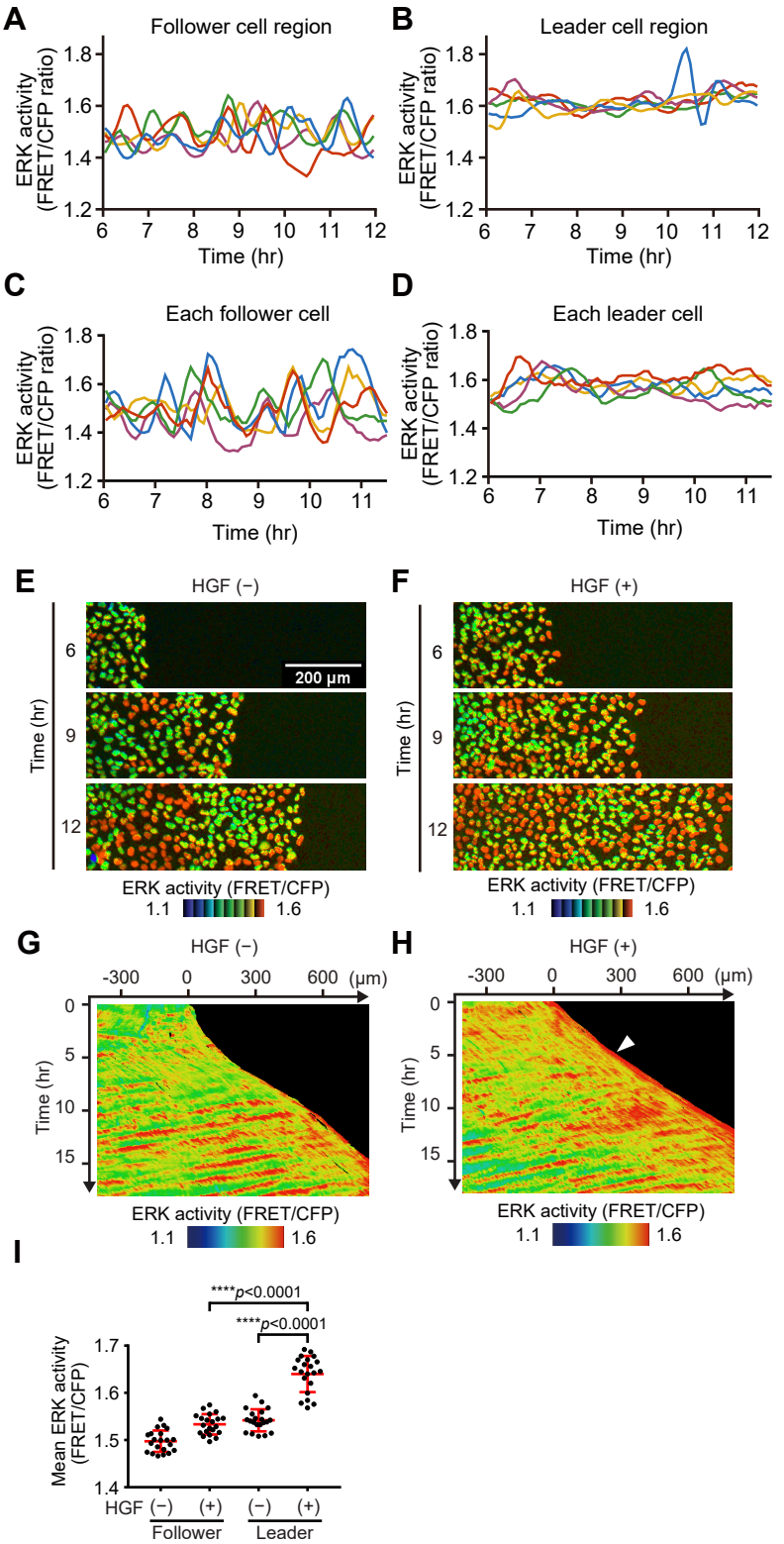

Figure S2. Different ERK activity dynamics in leader and follower cells, Related to Figures 1 and 2

(A and B) Temporal changes of ERK activity in five representative regions for each follower (A) and leader (B) cell region are plotted versus time after the start of imaging. The time-series data were processed by the moving average with a 15 min time window to reduce the noise.

(C and D) Temporal changes of ERK activity obtained by single-cell tracking with TrackMate in five representative cells for each follower (C) and leader (D) cell are plotted versus time after the start of imaging. The time-series data were processed by the moving average with a 15 min time window to reduce the noise.

(E-I) Images of ERK activity in serum-free media without (E) or with 2.5 ng mL^{-1} HGF (F) are represented at 6, 9, 12 hr after the start of imaging. (G and H) Kymographs of the ERK activity without (G) or with 2.5 ng mL^{-1} HGF (H) in (E) and (F), respectively. The white arrow head indicates the leader cell region showing sustained ERK activation. (I) Mean ERK activities in the follower and the leader cell regions from 5 to 18 hr after the start of the imaging. The red bars represent the means and SDs. Dunnett's T3 multiple comparisons test, n = 21 from three independent experiments.

Figure S3

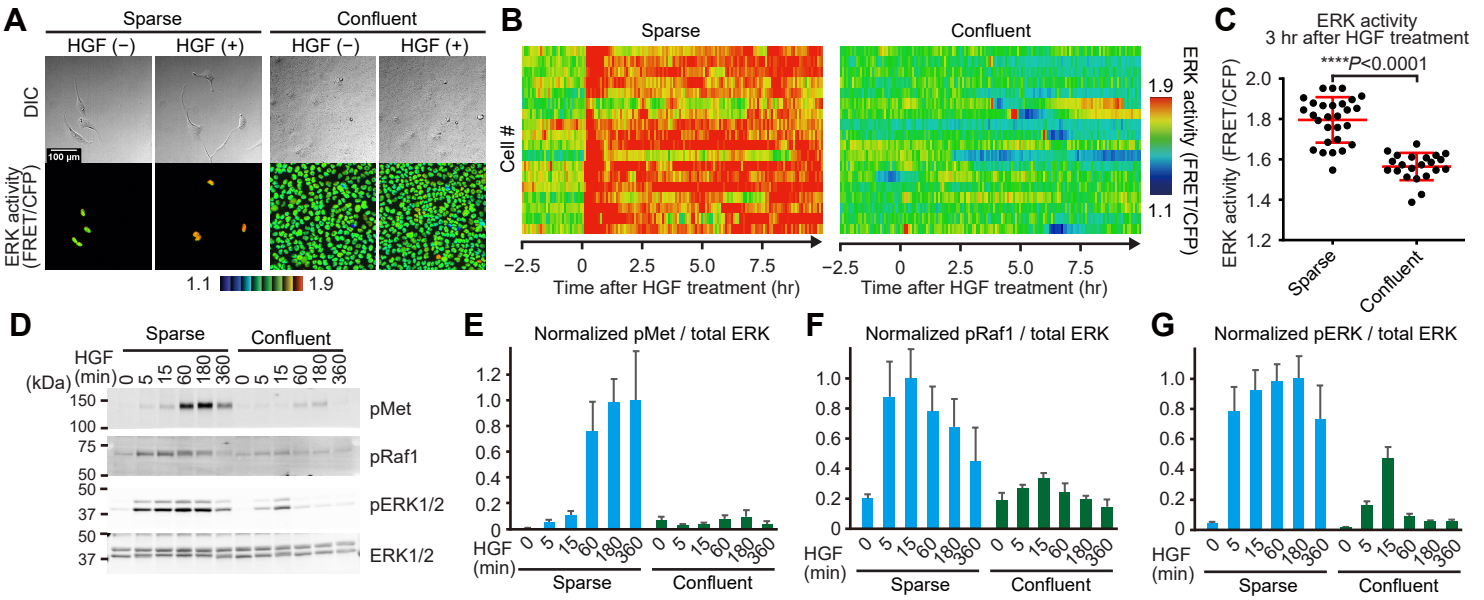

Figure S3. Cell density-dependent Met activation by HGF, Related to Figure 3

(A) MDCK cells expressing EKARrEV-NLS were seeded into a culture insert at a sparse or confluent condition in the FBS-free media containing 2 μM PD153035 (EGFR inhibitor). Cells were treated with 2.5 ng mL^{-1} HGF. Images are at immediately before (HGF (−)) and 3 hr after the HGF treatment (HGF (+)).

(B) Heatmaps of ERK activity in sparse and confluent cells (18 cells for each). Each row of the heatmaps represents single cell.

(C) ERK activities in sparse or confluent cells 3 hr after the HGF treatment are represented as dots. The red bars represent the means and SDs of the values. Welch' s t-test, n = 28 cells (sparse) and 22 cells (confluent) from two independent experiments.

(D) Sparse and confluent cells were treated with 2.5 ng mL^{-1} HGF in the presence of 2 μM PD153035 (EGFR inhibitor) and then lysed at the indicated time points. The cell lysates were analyzed by immunoblotting with the indicated antibodies.

(E–G) Normalized phosphorylation levels of Met (E), Raf1 (F), and ERK1/2 (G) are represented as means with SDs (n = 3).

Figure S4

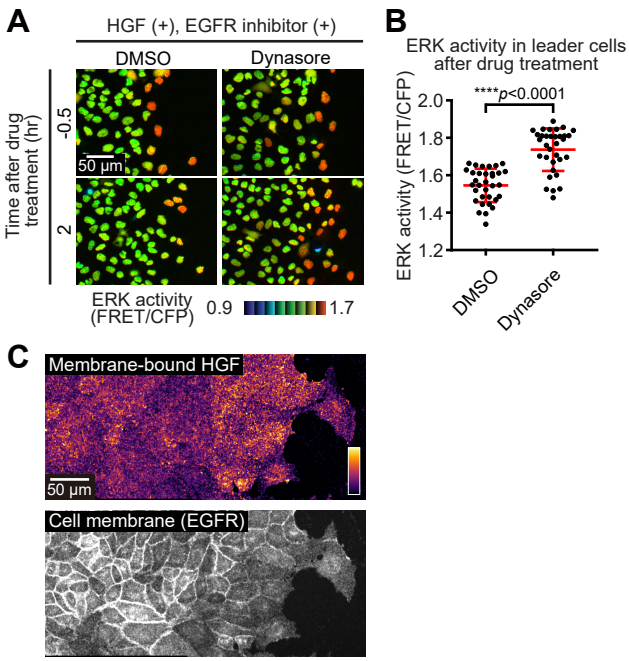

Figure S4. Similar binding of HGF to leader and follower cells, Related to Figure 3

(A and B) MDCK cells expressing EKARrEV-NLS were subjected to confinement release assay in the FBS-free media containing 2.5 ng mL^{-1} HGF and 2 μM PD153035. Cells were treated with 0.1% DMSO (left) and 80 μM Dynasore (right) 3.5 hr after the start of imaging. (A) Images −0.5 (upper) and 2 hr (lower) after the drug treatment are shown. (B) ERK activities in the leader cells 2 hr after the drug treatment are represented as dots. Welch' s t-test, n = 33 from three independent experiments.

(C) MDCK cells were subjected to confinement release assay in the FBS-free medium. The cells were treated with 20 ng mL^{-1} Rhodamine-HGF in the presence of 2 μM PD153035 6 hr after the start of migration on ice. The cells were fixed and subjected to immunofluorescence of EGFR. The upper and lower images indicate z-projection of Rhodamine-HGF and EGFR signals by summation of slices.

Figure S5

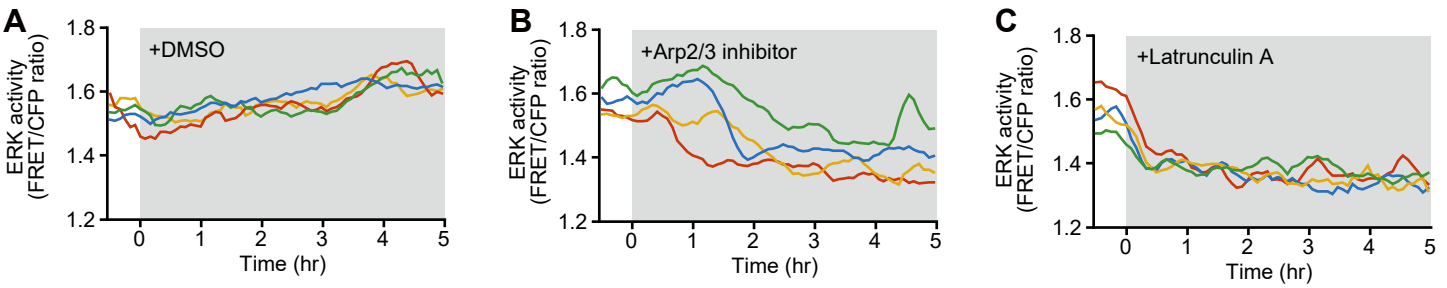

Figure S5. Decreased ERK activity after the inhibition of lamellipodial extension, Related to Figure 5

(A–C) Temporal changes of ERK activity upon 0.1% DMSO (A), 100 μM CK666 (Arp2/3 inhibitor; B), or 1 μM Latrunculin A (C) treatment obtained by single-cell tracking with TrackMate in four representative leader cells were plotted. The time-series data were processed by the moving average with a 15 min time window to reduce the noise.

Figure S6

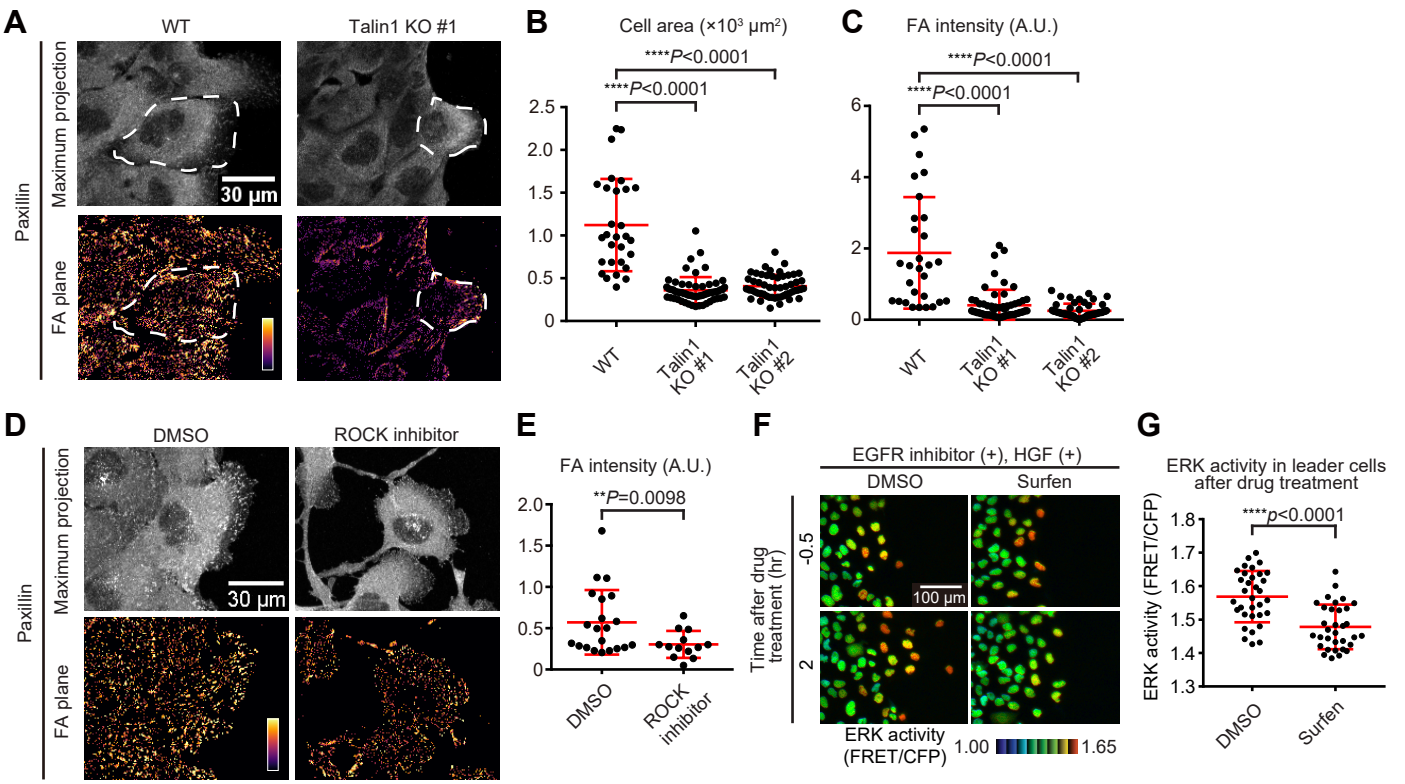

Figure S6. Decreased cell area and focal adhesions in Talin1 KO cells, Related to Figure 6

(A) Wild type MDCK cells and talin1 KO MDCK clone #1 cells were subjected to confinement release assay in the FBS-free medium containing 2.5 ng mL^{-1} HGF. The cells were fixed at 6 hr after the start of migration, and immunostained with anti-paxillin antibody. The upper images indicate maximum projections of the intensity. The lower images represent paxillin intensity at the basal plane.

(B) The cell areas of WT and talin1 KO leader cells are represented as dots. The red bars represent the mean and SDs of the values. Dunnett's T3 multiple comparisons test, n = 29 cells (WT), 60 cells (talin1 KO clone #1), and 53 cells (talin1 KO clone #2) from three independent experiments.

(C) The paxillin intensities at focal adhesions in WT and talin1 KO leader cells are represented as dots. Dunnett's T3 multiple comparisons test, n = 29 cells (WT), 60 cells (talin1 KO clone #1), and 53 cells (talin1 KO clone #2) from three independent experiments.

(D and E) MDCK cells were subjected to confinement release assay in the FBS-free medium containing 2.5 ng mL^{-1} HGF and 2 μM PD153035, and further treated with 0.2% DMSO or 30 μM Y27632 (ROCK inhibitor) at 3 hr after the start of migration. The cells were then fixed at 6 hr after the start of migration, and immunostained with anti-paxillin antibody. (D) The upper images indicate maximum projections of the intensity. The lower images represent paxillin intensity at the basal plane. (E) The paxillin intensities at focal adhesions in leader cells are represented as dots. Welch' s t-test, n = 21 cells (DMSO) and 13 cells (ROCK inhibitor) from three independent experiments.

(F and G) MDCK cells expressing EKARrEV-NLS were subjected to confinement release assay in the FBS-free media containing 2.5 ng mL^{-1} HGF and 2 μM PD153035. (F) Images before and 2 hr after the 0.1% DMSO (left) or 20 μM surfen (right) treatment are shown. (G) ERK activities in the leader cells 2 hr after the drug treatment are represented as dots. Welch' s t-test, n = 33 from three independent experiments.

Figure S7

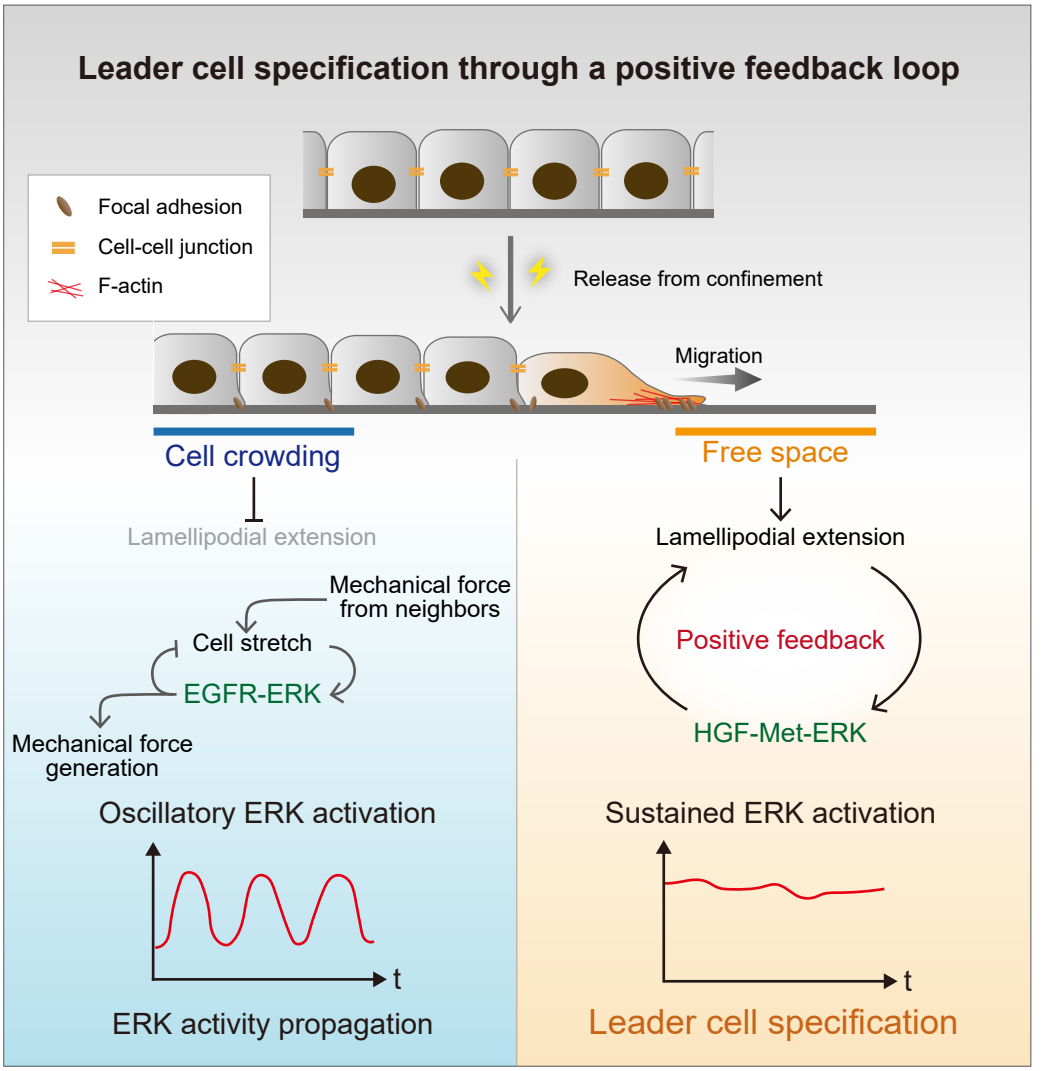

Figure S7. A positive feedback loop in leader cell specification during collective cell migration of epithelial cells, Related to Discussion
Upon the wounding or the removal of physical confinement, cells at the periphery of the epithelial cell sheet spread toward the free space. The lamellipodial extension increases the cellular HGF responsiveness, leading to sustained Met-ERK activation. The ERK activation further promotes the lamellipodium formation, giving rise to a positive feedback loop between lamellipodial extension and HGF-Met-ERK signal activation, and thereby ensuring the leader cell formation at the free edge of migrating cells. By contrast, follower cells show low HGF responsiveness due to the suppression of the lamellipodial extension by cell crowding. The oscillatory ERK activation in follower cells depends on the EGF-EGFR signaling pathway and is coupled with mechanical force generation, contributing to intercellular propagation of ERK activation and thus transferring the directional information.